2023

On the Chronological Understanding of the Homogeneous Dielectric Barrier Discharge

Xinpei Lu
Huazhong University of Science and Technology

Zhi Fang
Nanjing Tech Technology

Dong Dai
South China University of Technology

Tao Shao
Chinese Academy of Sciences

Feng Liu
Nanjing Tech Technology

See next page for additional authors

Original Publication Citation

Lu, X., Fang, Z., Dai, D., Shao, T., Liu, F., Zhang, C., Liu, D., Nie, L., & Jiang, C. (2023). On the chronological understanding of the homogeneous dielectric barrier discharge. *High Voltage*, *8*(6), 1132-1150. https://doi.org/10.1049/hve2.12382

Received: 23 April 2023 | Revised: 10 July 2023 | Accepted: 17 July 2023

High Voltage

DOI: 10.1049/hve2.12382

国家电网 STATE GRID 中国电力科学研究院有限公司 CHINA ELECTRIC POWER RESEARCH INSTITUTE | The Institution of Engineering and Technology | WILEY

REVIEW

On the chronological understanding of the homogeneous dielectric barrier discharge

Xinpei Lu[1] | Zhi Fang[2] | Dong Dai[3] | Tao Shao[4] | Feng Liu[2] | Cheng Zhang[4] | Dawei Liu[1] | Lanlan Nie[1] | Chunqi Jiang[5,6]

[1]State Key Laboratory of Advanced Electromagnetic Engineering and Technology, School of Electrical and Electronic Engineering, Huazhong University of Science and Technology, Wuhan, China

[2]College of Electrical Engineering and Control Science, Nanjing Tech Technology, Nanjing, China

[3]School of Electric Power, South China University of Technology, Guangzhou, China

[4]Institute of Electrical Engineering, Chinese Academy of Sciences, Beijing, China

[5]Frank Reidy Research Center for Bioelectrics, Old Dominion University, Norfolk, Virginia, USA

[6]Department of Electrical and Computer Engineering, Old Dominion University, Norfolk, Virginia, USA

Correspondence
Xinpei Lu.
Email: luxinpei@hotmail.com

Associate Editor: Dunpin Hong

Funding information
National Natural Science Foundation of China, Grant/Award Number: 52130701, 51977096, 12005076; National Key Research and Development Program of China, Grant/Award Number: 2021YFE0114700; Air Force Office of Scientific Research of the United States of America, Grant/Award Number: FA9550-22-1-0115, FA9550-22-1-0428

Abstract

Dielectric barrier discharges (DBD) are widely utilised non-equilibrium atmospheric pressure plasmas with a diverse range of applications, such as material processing, surface treatment, light sources, pollution control, and medicine. Over the course of several decades, extensive research has been dedicated to the generation of homogeneous DBD (H-DBD), focussing on understanding the transition from H-DBD to filamentary DBD and exploring strategies to create and sustain H-DBD. This paper first discusses the influence of various parameters on DBD, including gas flow, dielectric material, surface conductivity, and mesh electrode. Secondly, a chronological literature review is presented, highlighting the development of H-DBD and the associated understanding of its underlying mechanisms. This encompasses the generation of H-DBD in helium, nitrogen, and air. Lastly, the paper provides a brief overview of multiple-current-pulse (MCP) behaviours in H-DBD. The objective of this article is to provide a chronological understanding of homogeneous dielectric barrier discharge (DBD). This understanding will aid in the design of new experiments aimed at better comprehending the mechanisms behind H-DBD generation and ultimately assist in achieving large-volume H-DBD in an air environment.

1 | INTRODUCTION

Non-equilibrium atmospheric pressure plasma (N-APP) is a promising technology for generating high concentration reactive species at a relatively low gas temperature or room temperature [1–8], making it highly attractive for a variety of applications such as surface modification, decontamination of temperature-sensitive materials, and more [9–15]. Among the different methods used for generating N-APP, dielectric barrier discharge (DBD) is one of the most widely studied techniques and has been explored for more than a century [16–22]. In DBD, one or two dielectrics are inserted into the discharge circuit, which requires ignition of the discharge using alternating-current (AC) voltage or pulsed direct-current (DC) voltage. In addition to applying DBD for ozone generation [23–25], it has also been used for other applications including VUV sources, gas laser pumping, plasma displays, material processing, and plasma sources for medical uses [26–35]. The configuration of DBD can be broadly classified into two categories: surface DBD and volume DBD, and more

information about these configurations can be found in references [36, 37].

It was not until 1988 when Okazaki's group reported the generation of homogeneous plasma in helium (He) mixed with diluted oxygen at atmospheric pressure that DBD had been believed to occur only in a filamentary mode, where many short (<100 ns), narrow (<100 μm) current filaments are randomly distributed in time and space over the dielectric surface [38]. Soon after, many research groups worldwide became interested in generating homogeneous DBD (H-DBD), that is, plasma is uniform in any plane parallel to the electrode surface. Among the early works, Massines's group in France improved the understanding of the H-DBD mechanisms and demonstrated its applications on surface treatment and thin film coatings [39–42]. During that period, Roth's group in the United States also proposed many possible applications of DBD [43–45]. In the subsequent decades, atmospheric pressure H-DBDs have been generated and used for other applications [32, 46–53] with the mechanisms of H-DBDs better understood.

In short, DBD has been under investigation for decades; however, numerous unanswered questions remain. One particular example pertains to the proposed theory on N_2 homogeneous DBD, which suggests that generating a homogeneous DBD in the air is a difficult task [54–60]. This is due to the high concentration of O_2, which swiftly extinguishes the metastable state of N_2, within a timeframe much shorter than the period between consecutive discharges. The objective of this article is to provide a chronological understanding of homogeneous dielectric barrier discharge (DBD). This understanding will aid in the design of new experiments aimed at better comprehending the mechanisms behind H-DBD generation and ultimately assist in achieving large-volume H-DBD in an air environment.

2 | EFFECT OF VARIOUS PARAMETERS ON DBD

Before delving into the effects of various parameters on DBD, there are a few points that need clarification. Firstly, it should be noted that for most H-DBD configurations, a plate-plate electrode is used. Therefore, this paper will exclusively focus on DBD with a plate-plate electrode configuration.

Secondly, from a literal standpoint, a homogeneous DBD (H-DBD) indicates that the plasma is uniform. One of the most straightforward ways to differentiate between H-DBD and filamentary DBD (F-DBD) is to take photographs of the plasma. However, since most DBD is driven by kHz power supplies, and each discharge pulse lasts from tens of nanoseconds to tens of microseconds, photographs taken with regular commercial cameras may appear homogeneous due to the integration of many filamentary discharges. Therefore, to confirm whether a discharge is homogeneous or filamentary, high-speed intensified charge coupled device (ICCD) cameras are necessary. Early studies have suggested that a discharge is homogeneous if there is only a single current pulse per half cycle. However, in the case of an arc or spark discharge, a large current pulse does not prove the H-DBD, and high-speed photographs have shown that the plasma is in fact F-DBD [61].

Thirdly, H-DBD has two distinct modes: the Townsend DBD (T-DBD) and the glow-like DBD (G-DBD). In T-DBD, the luminous regime is next to the anode, while in G-DBD, a luminous region is next to the cathode. If the gap is large enough, a positive column can also be observed [39–42]. More details on the differences between T-DBD and G-DBD will be discussed later in the paper.

Lastly, in the following sections, we will discuss the effects of gas flow, dielectric material properties, surface conductivities, and electrode shape on the appearance of DBD.

2.1 | Effect of gas flow

In 2001, Gherardi and Massines [62] conducted a study on N_2 discharge in a 1 mm gap. They varied the N_2 flow velocity between 0 and 285 cm/s and used an AC power supply with a frequency range of 200 Hz to 20 kHz to drive the DBD. The study found that the formation of an H-DBD is primarily limited by the species etched from the surface, which act as quenchers of the $N_2(A)$ and can cause a transition from a homogeneous to filamentary discharge. The higher the amplitude or the frequency of the applied voltage is, the more the quenchers due to the etching are, that is reason of that there is an up limit of the amplitude and the frequency of the applied voltage for H-DBD.

However, Wang's group [63] later argued in 2010 that gas flow significantly decreases the density of $N_2(A)$ quenchers, particularly O_2 etching from the dielectric, resulting in a much higher $N_2(A)$ flux to the dielectric and release of trapped electrons on the surface. This process ultimately leads to the generation of H-DBD. Gherardi and Massines [62] believed that seed electrons were created within the gap through Penning ionisation between two N_2 metastables.

2.2 | Effect of dielectric material

The effect of dielectric material on the discharge mode of N_2 discharge was also conducted by Gheradi and Massines in 2001 [62]. They compared the discharge properties of an 8 μm thick polypropylene film deposited on both 635 μm thick Al_2O_3 plates to that of Al_2O_3 plates alone. Their results show that the H etching from polypropylene surfaces are more efficient in quenching N_2 metastables than those from alumina surfaces, which mainly consisted of O.

In 2008, Li et al. [64] studied the effect of different dielectric materials on DBD at reduced pressure air plasma. They used polytetrafluoroethylene (PTFE), quartz, and Al_2O_3 as dielectric plates and found that the pressure range for generating H-DBD was wider when using PTFE as the barrier. According to the surface charge measurement as shown in Figure 1, it can be seen that the trapped surface charge is the highest and decays slowest for PTFE. In addition, the thermal stimulated current (TSC) measurement results presented in Figure 2 show that the integration of TSC over temperature is also the highest for PTFE, and its trap centre is 0.37 eV. All these indicate that the high concentration of surface charge is trapped in the shallow trap,

which could provide a high concentration of seed electrons for homogeneous discharge. Again, also in 2008, Li et al. [65] used a corona discharge plasma to silicone rubber plates for different treatment times, it was found that the longer the treatment time, the higher the physical defects and the chemical defects observed by scanning electron microscopy and Fourier transform infrared spectroscopy methods. By using these corona discharge rubber plates in DBD, it is found that H-DBD can be obtained in a wider pressure range when the rubber plate has higher physical and chemical defects.

In 2018, Zhang's group [66] compared the discharges of Al_2O_3 and AlN dielectric plates using He/O_2 (0.2%–1%) as the working gas, a 2 mm gap distance, and a 20 kHz AC power supply to drive the plasma. They found that H-DBD could be obtained under certain ranges of applied voltage and O_2 percentage when using AlN as the dielectric. To understand the mechanism behind, the surface potential decay of the Al_2O_3 and AlN plate is measured, which is related to the surface residual charge deposited on the dielectric surface. It is found that the potential of AlN dielectric decays much slower. According to the energy distribution of the electron traps, the electron traps of AlN dielectric mainly distribute at the energy level of 0.92–1.02 eV, which is higher than that of Al_2O_3. Besides, the peak value of the trap density of AlN is also higher than that of Al_2O_3. This was believed to be the reason of obtaining H-DBD when AlN is used. However, how the trapped electrons are released was not discussed by the authors.

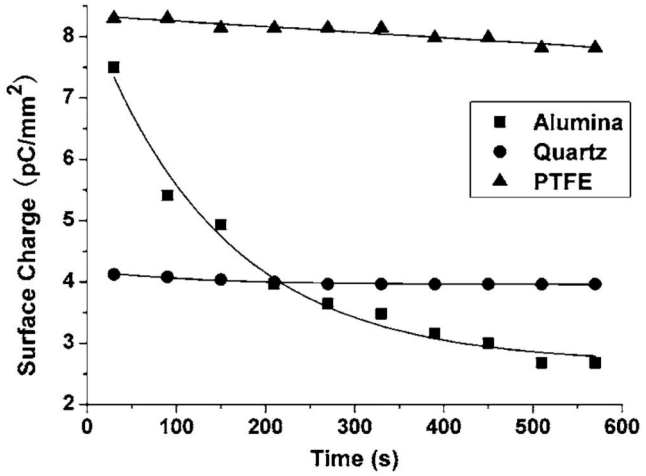

FIGURE 1 The results of the surface charge measurement. 2.5 mm air needle-plane geometry gap with a negative voltage of 5 kV corona discharge for 10 s [64].

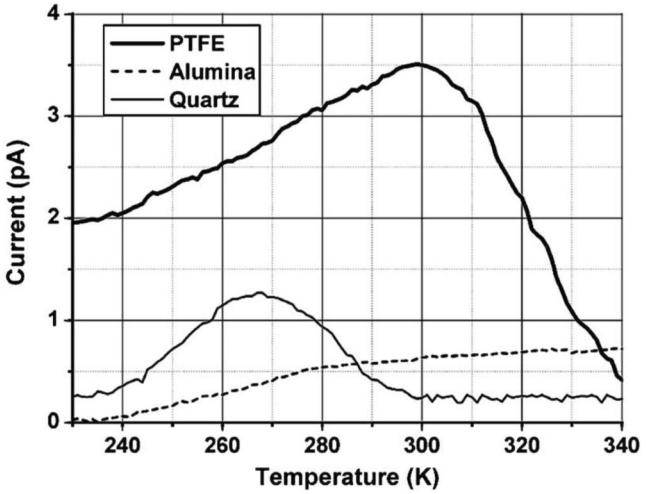

FIGURE 2 The results of thermally stimulated current measurement. The initial temperature was lowered to 200 K [64].

In another study in 2018, Ran et al. [21] investigated the effect of surface roughness on H-DBD. They found that using an Al_2O_3 dielectric with a surface roughness (R_a) of 288 nm and a thickness of 2 mm with a 1 kHz AC power supply could generate H-DBD in a 3 mm air gap. However, when the surface roughness was 100 nm or lower, the plasma was always filamentary even at a 1 mm air gap. This was attributed to the fact that rougher surfaces had more shallow traps to trap more seed electrons, and the higher local electric field enhancement reduced the breakdown electric field strength, making it easier to generate H-DBD. So H-DBD can be obtained when the roughness of the surface is higher.

2.3 | Effect of surface conductivity

In 2008, Naude and Massines [67] conducted a study on the homogeneity of a 3 mm gap DBD in argon (Ar) mixed with a few hundred ppm (part per million) of ammonia. Their experimental setup involved using a silicon wafer with a conductivity of 1 Ω·cm to cover one of the dielectric surfaces. The results showed that when the silicon wafer served as the anode, the plasma exhibited homogeneous discharge. However, when it was used as the cathode, filamentary discharge was observed. The authors attributed this phenomenon to the difference in surface conductivity. When the surface had low conductivity, a microdischarge caused a significant decrease in the gap voltage where the microdischarge appeared because the charges only deposit locally on a small area. So the deposited charges will induce a high reverse electric field. Conversely, when the surface had high conductivity, the charges spread over the entire substrate surface, leading to a small local electric field induced by the discharge that could not stop the microdischarge.

2.4 | Effect of mesh electrode

In 1993, Okazaki et al. [68] proposed the use of a fine metal wire mesh (diameter 0.035 mm) as an electrode and a polyethylene terephthalate (PET) plate as the dielectric. This setup was found to generate a homogeneous discharge in Ar, air, or N_2 at a gap distance of a few millimetres, using a 50 Hz AC voltage.

In 1998, Trunec et al. [69] also investigated the effect of the mesh electrode on He, Ar, and N_2 discharge in a 1.5 mm discharge gap using a 50 Hz AC power supply. They found that at a relatively low applied voltage, a homogeneous discharge could be obtained for all three types of gases. To better

understand the effect of the mesh electrode, they calculated the electric field distribution in the gap and found that the addition of mesh did not affect the electric field in the discharge. Furthermore, they estimated the resistance of the mesh to be about 0.5 Ω. They concluded that this resistance might prevent micro-discharge, resulting in the generation of H-DBD.

In 2006, Wang et al. [70] reported a homogeneous air DBD with a gap distance of 2 mm by using a mesh electrode with a wire diameter of 0.03 mm placed on a 0.1 mm thickness PET plate driven by a 50 Hz AC power supply. They calculated the electric field along the axis with an applied voltage of 6.6 kV, as shown in Figure 3. The results showed that the electric field next to the PET film was enhanced when a mesh electrode was used. This enhanced electric field could initiate corona discharge and provide seed electrons, which was proposed as the reason for generating H-DBD. It should be noted that reported by Trunec et al. [69], 1 mm Al_2O_3 was used, which is 10 times thicker than what was used by Wang et al. [70]. Although the dielectric constant of Al_2O_3 is about 9–10, which is larger than that of PET film of 3.8. But the PET film used by Wang et al. [70] is 10 times thinner than Al_2O_3 sheet used by Trunec et al. [69]. This may be the reason why Trunec et al. [69] did not observe electric field distortion in the gap by the mesh electrode.

3 | CHRONOLOGICAL UNDERSTANDING OF THE MECHANISM OF H-DBD

3.1 | He H-DBD

(1) Basic three conditions hypothesis

In 1990, Okazaki's group [71] proposed a set of rules for obtaining homogeneous DBD, which comprised three conditions. The first condition required the use of helium (He) as the dilute gas, which was believed to have high-energy metastable states (around 20 eV) that could ionise trace amounts of air in the gap, thus providing a longer glow-arc transition time. The second condition required the use of a high-frequency source, such as kHz or RF, although the authors did not provide a reason for this. They only described that atmospheric G-DBD was obtained in an 8 mm gap with He as the working gas and a 3 kHz power supply. The third condition involved covering at least one of the electrodes with a dielectric plate, which was attributed to the charge build-up on the dielectric plate resulting in an opposite voltage that would stop the discharge. The authors also obtained the cathode fall of the plasma based on the relation between the voltage and gap distance and confirmed that the plasma was G-DBD. However, the rules did not include a gap distance requirement, and the plasma could transition to F-DBD when the gap distance exceeded 8 mm. The same group also generated H-DBD in an Ar/NH_3 mixture [72]. NH_3 was added to Ar because the metastable state of Ar has an energy higher than the ionisation potential of NH_3. The use of Ar or other gases without He could also achieve H-DBD when the applied voltage frequency is sufficiently high. Therefore, the conditions for the generation of H-DBD need to be reevaluated.

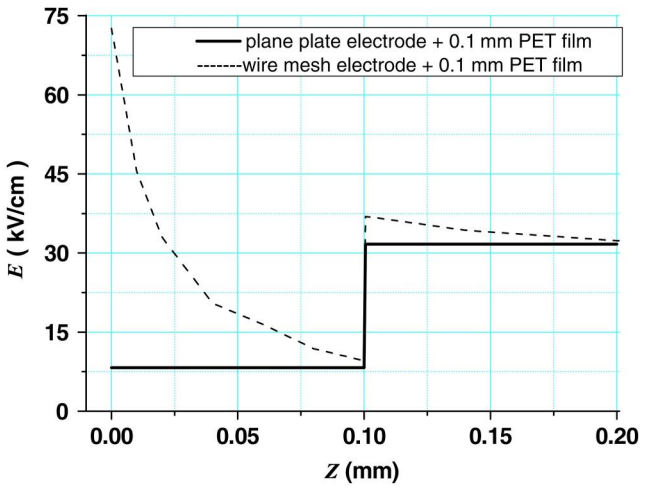

FIGURE 3 The electric field in a 2 mm air gap. Z = 0 and Z = 0.1 mm is the electrode-PET interface and PET-air gap interface, respectively. Applied voltage 6.6 kV, frequency 50 Hz AC [70].

(2) Advanced three conditions hypothesis

In 1998, Massines and colleagues [39] investigated a 5 mm gap dielectric barrier discharge (DBD) driven by a 10 kHz AC power supply with He as the working gas. Their results showed that between two consecutive discharges, the current is not equal to 0, and there is a small "residual current peak" when the gas voltage reverses, which decreases with a decrease in the frequency of the applied voltage to lower than 5 kHz or when trace amounts of air are present. To understand this observation, they carried out one-dimensional modelling and added 0.5% N_2 to He to mimic the roles of He impurities. Their simulation successfully reproduced the current behaviour between two consecutive discharges as shown in Figure 4. The simulated spatial and temporal resolved electron density distribution showed that when the polarity of the gap voltage changes, the electrons move to the new anode, which is related to the current peak around the time when the polarity of the gas voltage changes.

The plasma generated by the discharge was also captured by a high-speed ICCD camera and reported for the first time, as shown in Figure 5 [39]. It clearly indicates that the discharge is a glow DBD. This was also confirmed by their one-dimensional simulation, where the cathode fall, negative glow, Faraday dark space, and positive column region can be clearly seen.

Based on their observation, they proposed the following three-condition hypothesis for the generation of atmospheric pressure H-DBD. Firstly, the breakdown electric field E_{bd} must be low to control the avalanche amplification and avoid it from

growing too fast. This can be achieved by having Penning ionisation as the main path of electron creation, which leads to an increase in the ionisation coefficient at low electric field. Secondly, the residual electron density in the gas before the ignition of a new discharge must be high enough, which is linked to the amplitude of the reverse current peak. They assumed that an electron density of at least 10^6–$10^7/cm^3$ is needed for H-DBD. This is the reason why the plasma transits to filamentary when the frequency of the applied voltage is too low because the residual electron density decays with time. Thirdly, the electrons trapped in the shallow traps of the dielectric surface during the previous current pulse also play an important role in obtaining an H-DBD.

To determine if Penning ionisation $He(2^3S) + N_2 \rightarrow N_2^+(B) + He + e$ can contribute enough ionisation, they compared the simulation on the direct ionisation (electron collision ionisation) and Penning ionisation, as shown in Figure 6 [73]. The two ionisation paths were found to be comparable.

Additionally, it should be noted that the $He(2^3S)$ contributed to the Penning ionisation is generated during the current pulse rather than from the previous pulse. This is because the lifetime of $He(2^3S)$ is shorter than the pulse period as can be seen from the following reactions,

$$He(2^3S) + He \rightarrow 2He + h\nu, \quad (1)$$

$$He(2^3S) + 2He \rightarrow He_2 + He, \quad (2)$$

$$He(2^3S) + e \rightarrow He + e, \quad (3)$$

where the reaction rate coefficients are $k_1 = 6.0 \times 10^{-15}\ cm^3s^{-1}$, $k_2 = 2.5 \times 10^{-34}\ cm^6s^{-1}$, and $k_3 = 2.9 \times 10^{-9}\ cm^3s^{-1}$, respectively [74–82]. The lifetime of $He(2^3S)$ was estimated to be on the order of tens of μs, when a trace amount of N_2 or O_2 is presented. The lifetime of $He(2^3S)$ could be even shorter. For example, when 1% of N_2 is presented, $He(2^3S) + N_2 \rightarrow He + N_2^+ + e$. This reaction has a reaction coefficient of $5 \times 10^{-17}\ m^3/s$. So $He(2^3S)$ has a lifetime of about 1 μs under such conditions.

Finally, the simulation on the electric field, ion density, and electron density spatial distribution by Massines et al., as shown in Figure 7, clearly shows that the plasma is a glow discharge, where the electric field next to the cathodes is high, corresponding to the cathode fall.

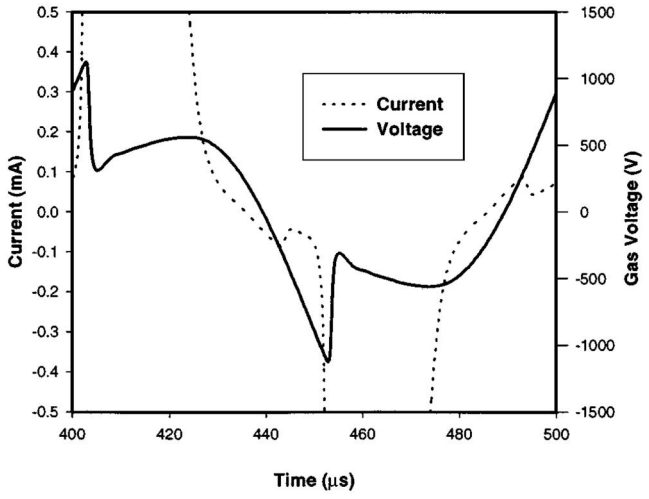

FIGURE 4 Time variation over one cycle of the low values of the calculated discharge current, and of the gas voltage. Gap distance: 5 mm. Working gas: He (99.5) + Ar (0.5%) [39].

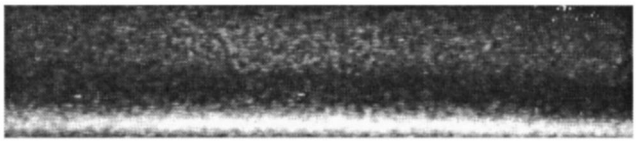

FIGURE 5 10 ns exposure time photograph of the 5 mm gap taken when the discharge current is maximum. The cathode is located at the bottom. Gap distance: 5 mm. Working gas: He [39].

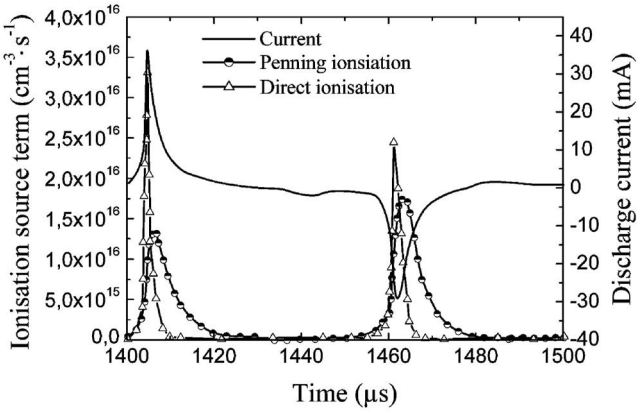

FIGURE 6 Calculated source terms of direct and Penning ionisation in an He H-DBD [73].

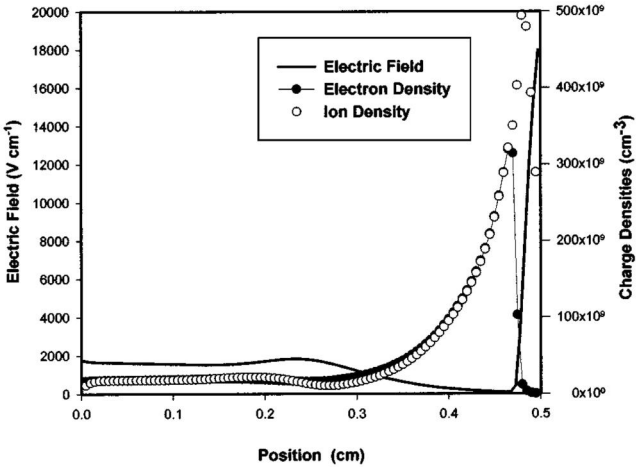

FIGURE 7 Spatial evolution of the electric field, the ion, and the electron densities at the time when the discharge current is maximum. Gap distance 5 mm, working gas He. The cathode is on the right-hand side and the anode on the left [39].

3.2 | N_2 H-DBD

(1) N_2 metastable Penning ionisation hypothesis

In 2000, Massines et al. [77] conducted a study on the behaviour of atmospheric pressure N_2 discharge with gap distances of a few mm. The results showed that as the dissipated power increased, a transition from homogeneous to filamentary mode was always observed. However, the minimum power required for this transition varied depending on the nature of the dielectric surface. This variation was attributed to the quenching rate of $N_2(A)$ by H, which was found to be about 10 times higher than that of O. The etching product of Al_2O_3 plate was mainly O, while that of polymer film was mainly H, allowing the former to operate in a homogeneous mode at high power and the latter only at low power.

Furthermore, the power deposited in an F-DBD was found to be greater than that of H-DBD, but the emission of NO_γ was much lower, and ON_2 was not even observed in F-DBD. The temporal emission behaviour of NO_γ, N_2, ON_2, and the discharge current as shown in Figure 8 suggested that NOγ was not excited by electrons (reaction 4) but by long lifetime, high-energy species, that is, $N_2(A)$ through reaction (5). Similarly, ON_2 was generated through reactions (6) and (7), which also required the participation of $N_2(A)$. Therefore, the concentration of $N_2(A)$ was significantly reduced in F-DBD [77].

Based on the above discussion, it was concluded that the H-DBD generated in N_2 was due to the high concentration of seed electrons generated through Penning ionisation between two N_2 metastable molecules via reactions (8) and (9).

$$\mathrm{NO}\left(\mathrm{X}\ ^2\prod_r\right)+\mathrm{e}\rightarrow\mathrm{NO}\left(\mathrm{A}\ ^2\sum^+\right)+\mathrm{e}, \tag{4}$$

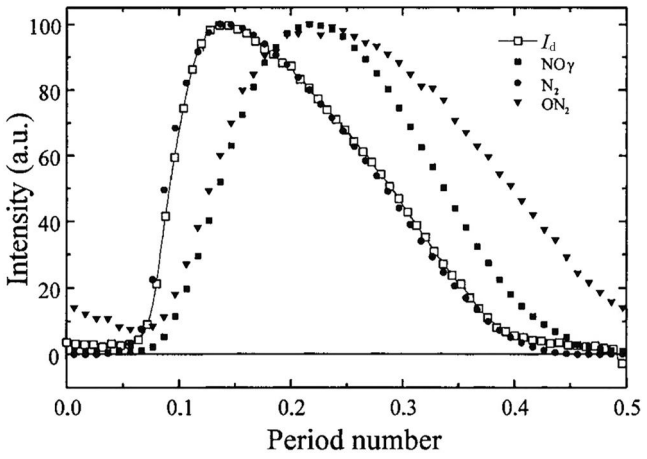

FIGURE 8 Time variation during a half-cycle of the discharge current (I_d) and the amplitude of the emission bands. The maximum of the current and the emission are normalised to 100, and the exposure time of each spectrum is 10 ns. The gas gap is 2 mm and the applied voltage has a peak of 8 kV [77].

$$\mathrm{NO}\left(\mathrm{X}\ ^2\prod_r\right)+\mathrm{N_2}\left(\mathrm{A}\ ^3\sum_u^+\right)\rightarrow\mathrm{NO}\left(\mathrm{A}\ ^2\sum^+\right)+\mathrm{N_2}\left(\mathrm{X}\ ^1\sum_g^+\right), \tag{5}$$

$$\mathrm{O}\left(^3\mathrm{P}\right)+\mathrm{N_2}\left(\mathrm{A}\ ^3\sum_u^+\right)\rightarrow\mathrm{O}\left(^1\mathrm{S}\right)+\mathrm{N_2}\left(\mathrm{X}\ ^1\sum_g^+\right), \tag{6}$$

$$\mathrm{O}\left(^1\mathrm{S}\right)+\mathrm{N_2}\left(\mathrm{X}\ ^1\sum_g^+\right)+\mathrm{N_2}\rightarrow\mathrm{O}\left(^1\mathrm{S}\right)\mathrm{N_2}+\mathrm{N_2}, \tag{7}$$

$$\mathrm{N_2}\left(\mathrm{a'}\ ^1\sum_u^-\right)+\mathrm{N_2}\left(\mathrm{A}\ ^3\sum_u^+\right)\rightarrow\mathrm{N_4^+}+\mathrm{e}, \tag{8}$$

$$\mathrm{N_2}\left(\mathrm{a'}\ ^1\sum_u^-\right)+\mathrm{N_2}\left(\mathrm{a'}\ ^1\sum_u^-\right)\rightarrow\mathrm{N_4^+}+\mathrm{e} \tag{9}$$

The respective reaction rates are $k_4 = 2.0 \times 10^{-10}\mathrm{cm^3s^{-1}}$ [83], $k_5 = 6.6 \times 10^{-11}\mathrm{cm^3s^{-1}}$ [79], $k_6 = 2.1 \times 10^{-11}\mathrm{cm^3s^{-1}}$ [80], $k_7 = 4 \times 10^{-18}\mathrm{cm^3s^{-1}}$ [81], $k_8 = 5 \times 10^{-11}\ \mathrm{cm^3s^{-1}}$ [82], and $k_9 = 2 \times 10^{-10}\ \mathrm{cm^3s^{-1}}$ [82].

(2) $N_2(A) + e_{trapped} \rightarrow N_2 + e$ hypothesis

Then few years later, in 2003, Massines's group [73] acknowledged that Penning ionisation between two metastable states (reaction 8 and 9) cannot contribute to the seed electrons required for H-DBD due to the short lifetime of $N_2(a)$. In an effort to confirm this, they added Xe to N_2, since Xe is an efficient quencher of $N_2(a)$ but not $N_2(A)$ [61]. Their findings indicated that H-DBD could still be obtained, thus supporting the notion that $N_2(a)$ does not play a significant role in the generation of H-DBD.

As a result, the group proposed that the $N_2(A)$ flux to the dielectric surface, which significantly increases the cathode secondary emission coefficient γ, is responsible for the H-DBD. This is illustrated in Figure 9, which depicts the group's simulation results showing that the $N_2(A)$ flux to the dielectric surface is comparable to the ion flux. It is therefore assumed that $N_2(A)$ generates seed electrons by removing the trapped electrons trapped in the shallow trap during the previous discharge.

Besides, their simulation results on the electric field, ion density, and electron density spatial distribution as shown in Figure 10 clearly show that the plasma is Townsend discharge, where it's electric field along the discharge is more or less uniform.

When Al_2O_3 was used as the dielectric, the quencher O_2 was believed to result from the etching of the dielectric surface. To better know the effect of O_2 on the transition of H-DBD to F-DBD, in 2005, Kozlov et al. [82] investigated the effect of trace amounts of O_2 on N_2 DBD driven at 6.5 kHz in a gap of approximately 1 mm. It was found that the plasma appeared as

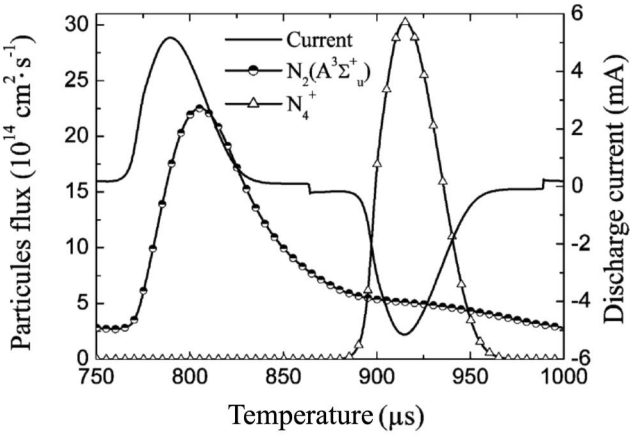

FIGURE 9 Discharge current, N_4^+ and $N_2(A)$ metastable fluxes on one of the dielectric surface as a function of time during a cycle in a H-DBD in N_2. The considered dielectric is on the anode during the first current peak and on the cathode during the second one [73].

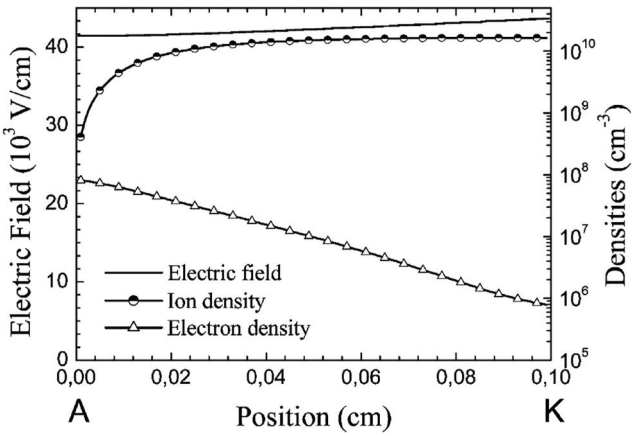

FIGURE 10 Calculated space distribution from the anode to the cathode of the electrical field, the ion and electron densities in a N_2 H-DBD when the discharge current intensity is maximum. Gap distance 1 mm [73].

a Townsend discharge when the O_2 concentration was below 500 ppm. However, when the O_2 concentration exceeded 1000 ppm, the discharge appeared in an F-DBD mode. This was attributed to the much more effective quenching of $N_2(A)$ by O_2, as can be seen from reactions (10) and (11). Brandenburg et al. [83] reported similar findings in the same year, noting that the H-DBD to F-DBD transition occurred at around 450 ppm O_2.

$$N_2(A) + N_2 \rightarrow N_2(X) + N_2, \quad (10)$$

$$N_2(A) + O_2 \rightarrow N_2(X) + O_2(a, b), \quad (11)$$

where $k_{10} = 3 \times 10^{-18}$ cm^{3}s^{-1} and $k_{11} = 2.54 \times 10^{-12}$ cm^{3}s^{-1}.

However, Kozlov et al. [82] observed a significant increase in N_2 second positive system emission when the O_2 concentration was increased from 0 to 40 ppm, as shown in Figure 11.

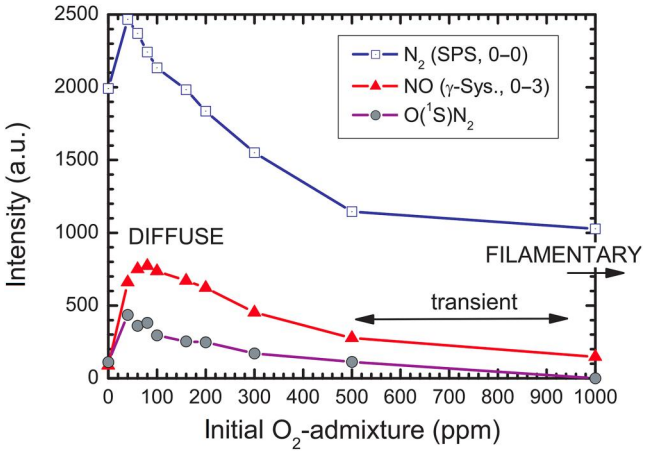

FIGURE 11 Transition between the filamentary and diffuse modes. Behaviour of the integral radiation intensities for selected species. Gap distance 1 mm, applied voltage 19 kV, frequency 6.5 kHz AC [82].

This observation cannot be explained by the current knowledge of DBD in N_2 and will be further discussed in the next section.

To better know the effect of $N_2(A)$ on DBD behaviour, in 2007, Dilecce et al. [83] reported the first temporal and spatial resolved measurement of $N_2(A)$ concentration in a N_2 with small O_2 admixture discharge by LIF. In their experiment, a trace amount of O_2 is added to the main working gas N_2. The gap distance is 1.4 mm, and the frequency of the applied voltage is 1.79 kHz. It was found that the H-DBD to F-DBD transition starts at 250 ppm O_2, but the $N_2(A)$ concentration during the discharge current pulse does not decrease dramatically when 250 ppm O_2 is added. The $N_2(A)$ concentration is on the order of 10^{13}/cm^3. However, the $N_2(A)$ decays much faster when O_2 is added due to the much higher quenching rate of O_2, O, and NO as shown in reactions (11)–(13).

$$N_2(A) + O \rightarrow N_2(X) + O(^1S), \quad (12)$$

$$N_2(A) + NO \rightarrow N_2(X) + NO, \quad (13)$$

where the reaction rate of Equations (12) and (13) are $k_{12} = 2.1 \times 10^{-11}$cm^{3}s^{-1} and $k_{13} = 7 \times 10^{-11}$cm^{3}s^{-1}, respectively.

(3) N(P) + O(P) → NO^+ + e hypothesis

As previously mentioned, Brandenburg et al. [84] reported an increase in plasma stability and N_2 second positive system emission when very low concentrations of O_2 (up to 40 ppm) were added, which could not be explained by current theory. To better understand this phenomenon, Tyl et al. [85] designed a specialised experiment setup. In their electrode configuration, the ground electrode was divided into eight disconnected strips (3.4 mm × 30 mm) with a 400 μm distance between nearby strips, and each strip was connected to a 1.7 kΩ resistor. The typical current and voltage waveform of the plasma is shown in

Figure 12. It is evident that there is a current component that changes sign immediately when the gas voltage polarity reverses. This was attributed to electrons continuously produced between two discharges because ions are heavy and the electric field is low, which cannot respond to the change of voltage polarity so quickly.

The evolution of the current jump (the sudden increase of the current when the voltage switch polarity) as a function of position for various O_2 concentrations is illustrated in Figure 13. The current jump increases significantly when 25 ppm O_2 is added, as evident from the plot. Further increase in O_2 concentration results in a decrease of the current jump, but it remains higher than the case of pure N_2 until the O_2 concentration reaches approximately 200 ppm. Subsequently, the current jump becomes lower than that of pure N_2, when 450 ppm O_2 is added, and a further increase in O_2 concentration, the transition to F-DBD occurs.

Figure 14 presents the optical emissions of N_2 Herman Infrared (N_2-HIR) system, NOγ, $O(^1S)N_2$, power deposited, and current jump as a function of O_2 concentration at the gas output (on the eighth strip). The N_2-HIR is due to reaction (14), while NOγ and $O(^1S)N_2$ are related to reactions (5)–(7). The decrease of N_2-HIR with an increase in O_2 concentration was attributed to the quenching of $N_2(A)$ by O_2. The current jump's increase when O_2 is increased from 0 to 50 ppm cannot be explained solely by $N_2(A)$ since $N_2(A)$ concentration actually decreases. Finally, it was proposed that the associative ionisation reaction between $N(^2P)$ and $O(^3P)$ is responsible for the current jump, as indicated by reaction (15), which is closely related to H-DBD, based on the increase in $O(^1S)N_2$ emission, which is related to $O(^3P)$ as can be seen from (5)–(7).

$$N_2(A) + N_2(A) \rightarrow N_2(C'') + N_2(X), \tag{14}$$

$$N(^2P) + O(^3P) \rightarrow NO^+ + e \tag{15}$$

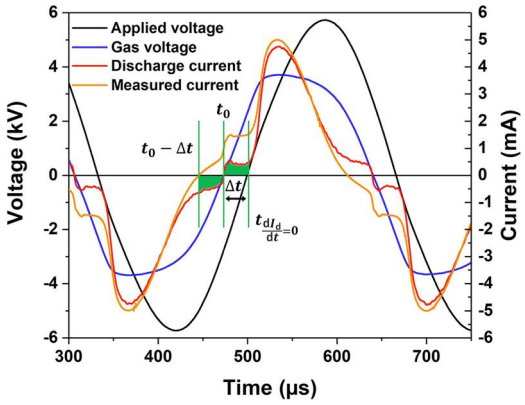

FIGURE 12 Oscillogram of a DBD in N_2 with 25 ppm O_2 (3 kHz, 11.6 kVpp, 1 mm) [85].

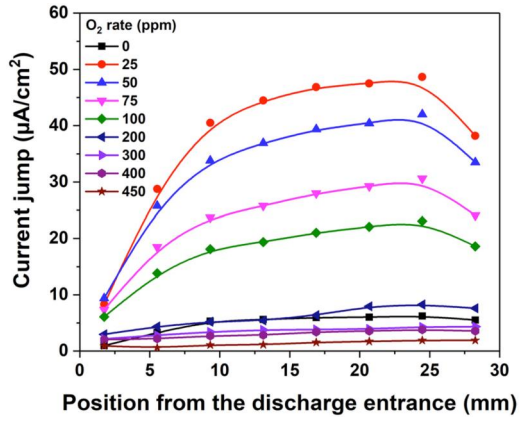

FIGURE 13 Current jump evolution as a function of the position in N_2 DBD with different concentration of O_2 (3 kHz, 12 kV_{pp}, 1 mm) [85].

3.3 | Ion trapping hypothesis

In 2005, Roth et al. [86] proposed the ion trapping mechanism for generating atmospheric pressure H-DBD. According to this mechanism, H-DBD can be obtained when the gap distance, electric field, and frequency are adjusted such that ions are trapped between the electrodes during an AC cycle, while electrons are free to travel to the electrodes. The frequency f_0 of the applied voltage should lie between certain limits given by Equation (14),

$$\frac{eU_{rms}}{\pi m_i v_{ci} d^2} \leq f_0 \leq \frac{eU_{rms}}{\pi m_e v_{ce} d^2} \text{ [Hz]} \tag{16}$$

where U_{rms} is the applied voltage, d is the gap distance, and m_e and m_i are the mass of the electron and ion, respectively.

In 2009, Massines et al. [61] pointed out that the ion density near the cathode in G-DBD is on the order of 10^9/cm^3, and its flux at the cathode is on the order of 10^{13}/(cm^2·s), as seen in Figure 7. This could result in a significant emission of electrons from the cathode. However, the ion density decreases with time, so if the excitation frequency is too low

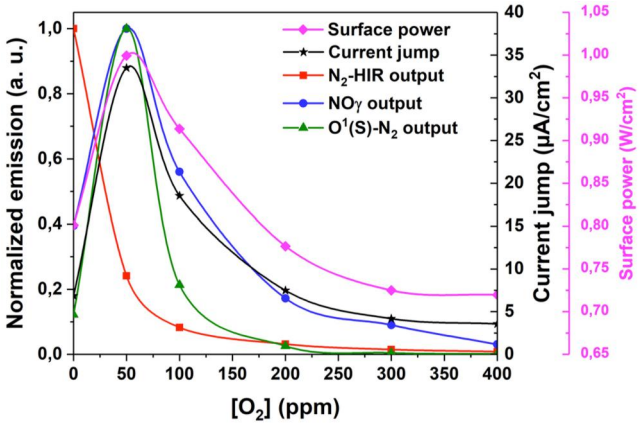

FIGURE 14 Correlation between the current jump, the surface power and N_2-HIR, NO_γ, $O(^1S)N_2$ emissions as a function of O_2 concentration, at the gas output on the eighth zone (3 kHz, 12 kV_{pp}, 1 mm) [85].

(typically <1 kHz), such a mechanism is not fulfilled. Besides, in T-DBD, there is no positive column, and the electric field in the gap is much higher, as shown in Figure 10. Ions drift to the cathode at a timescale of microseconds, and thus they do not contribute to H-DBD.

3.4 | Air H-DBD

For the low operation cost, air (mainly composed of nitrogen and oxygen) is considered as the most desirable working gas for industrial applications as shown in Figure 15. However, different from DBD in nitrogen, the nitrogen metastable species in air discharge would be efficiently quenched and electrons would also be easily attached to electronegative gases, such as oxygen and water vapour, which induces DBD in air usually in filamentary mode at atmospheric pressure. Therefore, after Okazaki's group first reported generating H-DBD in He in 1988 [38], it takes a few more years for them to report a H-DBD in air in 1993, which was generated by a 50 Hz AC voltage at gap distance of few mm with 0.035 mm diameter fine metal wire mesh electrode and a polyethylene terephthalate (PET) plate as the dielectric [68]. Inspired by the achievement of Okazaki's group, more researchers obtained H-DBD using mesh electrodes and electret materials [87–89]. With the development and application of pulsed power supplies for discharge excitation, short pulses exhibit the advantages in generating H-DBD in air [90–93].

(1) Electrode structure

Since Okazaki's group realised H-DBD in air by utilising mesh electrode and PET plate in 1993, Tepper et al. [87] and Fang et al. [88] realised H-DBD in nitrogen and air with the electret film and mesh electrode structure. The uniformity of the discharge with the mesh electrode covered by PET film was also first observed by ICCD with 100 ns exposure time. Fang et al. [94] investigated the factors, including voltage amplitude, gap distance, electrode configuration and barrier thickness, influencing the H-DBD in air and concluded that the important role of the wire mesh to provide initial electrons by producing corona discharge. Buchta et al. [89] proposed that the high resistance of the mesh electrode could inhibit the transition from uniform discharge to filamentary discharge. Golubovskii et al. [95] investigated the function of PET film in H-DBD by performing a two-dimensional fluid simulation and found the PET film as electret material could maintain the charge for a long time from the last discharge to the successive discharge as seed electrons. In 2013, Shao et al. [96] compared the metal electrode and water electrode air DBD as shown in Figure 15. For the metal electrode, the experimental results showed that the discharge was uniform at the 1 mm gap, and when the gap increased to 4 mm, the discharge changed into a filament mode. The discharge of water electrode always presented a uniform pattern. The water electrode could be regarded as a resistance in series with the discharge circuit. It acted as a distributed ballast to limit the discharge current, which also resulted in a lower rotating temperature of the water electrode compared with the metal electrode, thus avoiding the transition from glow to filament. In 2017, Liu et al. [97] proposed a line-plane electrode with floating voltage electrode, which was composed of high-voltage electrode, floating voltage electrode, air gap, barrier medium, and metal electrode. The research on the electric field of the line-plane electrode with floating voltage electrode showed that the strong electric field regions that were conducive to the initial discharge were

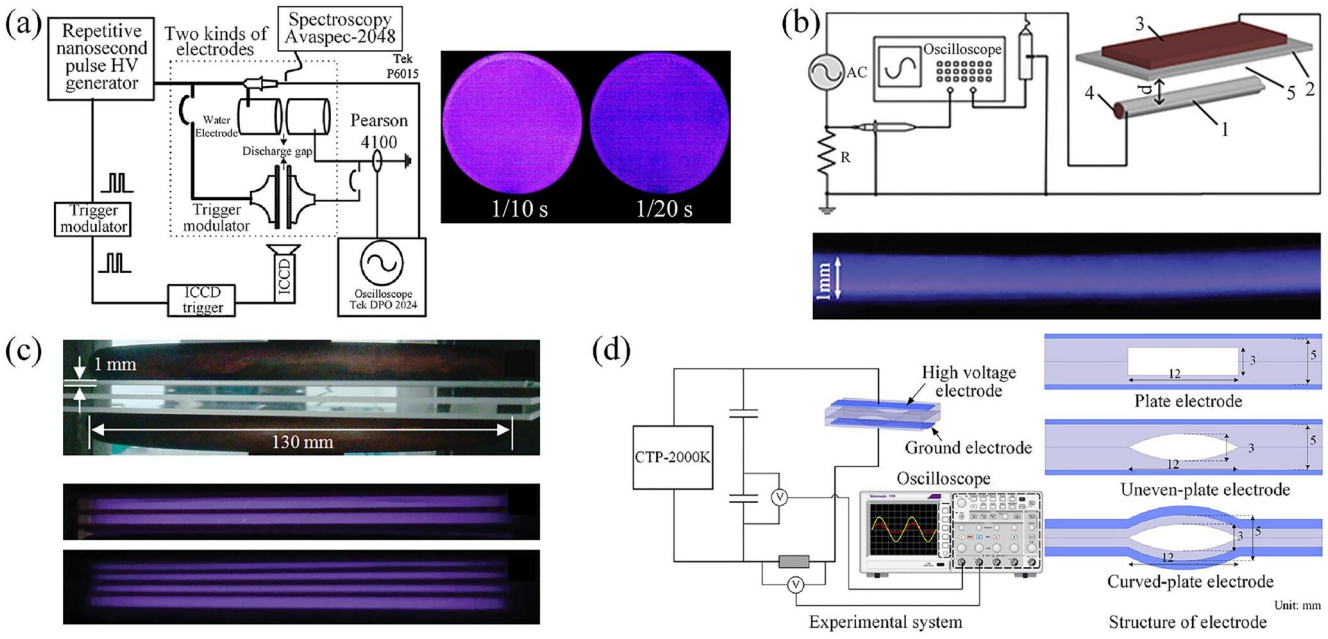

FIGURE 15 DBD experimental device (a) water electrode air DBD [96]; (b) floating voltage electrode DBD [97]; (c) multilayer DBD [98]; and (d) curved plate electrode DBD [99].

formed near the contact point between the high voltage electrode and the floating voltage electrode, and these regions could provide enough and uniformly distributed initial electrons for the air gap with relatively uniform and low electric fields. Therefore, the filament discharge could be suppressed. In 2018, Li et al. [98] reported a multilayer DBD structure driven by submicrosecond pulsed power for H-DBD in air generation. The H-DBD could be generated with different gas gaps and different thicknesses of dielectric. And the discharge uniformity is mainly determined by the distance of the larger gap. With more than 4 mm gas gap, the discharge stayed in a filamentary mode. In 2021, Cui et al. [99] realised the enhanced Townsend discharge in air with a curved plate electrode. Due to low discharge voltage and weak filament discharge intensity, the number of spikes in the current waveform of uneven plate electrode was reduced, and the spikes in the current waveform of curved plate electrode were almost eliminated. A certain degree of non-uniform electric field distribution could control the development of electron avalanche and adjust the transition from electron avalanche to streamer with non-uniform electric field distribution.

(2) Dielectric material

The dielectric material can affect the discharge mode by its surface characteristics and electric properties. Besides electret material, Osawa et al. [100] found that porous alumina ceramic played an important role in generating stable Townsend discharge. The "shallow trap" effect on the surface of alumina ceramics provides additional seed electrons and forms a uniform discharge in the air. Ran et al. [21, 101] studied the influence of dielectric surface morphology on discharge mode using different dielectric materials with similar equivalent capacitance and barrier media with surface morphology as shown in Figure 16. The results showed that the surface morphology of the dielectric materials played an important role in the discharge mode. With the quartz glass surface roughness increasing, the filaments decreased correspondingly. With a suitable surface roughness of alumina ceramic (R_a = 203 nm), the H-DBD in air could be obtained. Zhang et al. [102] found the emission intensity of N_2 ($C^3\Pi_u \rightarrow B^3\Pi_g$, 0-0, 337.1 nm) was almost proportional to the dielectric constant of the material, and the seed electrons required for uniform discharge could be generated by depositing absorbed electrons in shallow wells with energy levels lower than 1 eV. It would be easy to obtain uniform discharge using low dielectric constant dielectric plates. Belinger et al. [58] investigated the influence of the dielectric thickness on the homogeneity of H-DBD in air, which was related with the dielectric capacitance, and concluded that the H-DBD resulted from the control of the current density by the means of the dielectric capacitance.

(3) Power supply

Around 2000, most researchers powered DBD with 50 Hz power frequency AC power supply [68, 88, 103]. After 2010, high-frequency (such as 50 kHz) AC or pulsed power supplies became more popular power sources for generating H-DBD due to their identified advantages in applications [90, 93, 104]. Yang et al. [93] demonstrated the generation of H-DBD in nitrogen for an interelectrode gap distance of 4.5 mm and in air for a gap distance of 3.5 mm using a bipolar nanosecond pulsed voltage with 20 ns rise time. The gas temperature was found to be increasing with the gas-gap distance but almost constant with the pulse voltage (from 22 to 30 kV) or pulse repetition rate (from 90 to 210 Hz). Wang et al. [104] compared the discharge uniformity, power deposition, energy efficiency, and operation temperature between a coaxial DBD reactor driven by AC and nanosecond pulsed voltages. As shown in Figure 17a, the nanosecond pulsed coaxial DBD has a better discharge uniformity, a much higher instantaneous power deposition, and a higher energy efficiency with lower operation temperature. Jiang et al. [90] compared the DBDs generated by 40-kHz AC and 70-ns duration, 40-ns rise time nanosecond pulsed power supplies, as shown in Figure 17b. The comparative images indicate that the nanosecond-pulsed DBD behaves in a homogeneous mode, whereas the AC DBD consists of distributed filaments.

(4) Mechanisms for air H-DBD

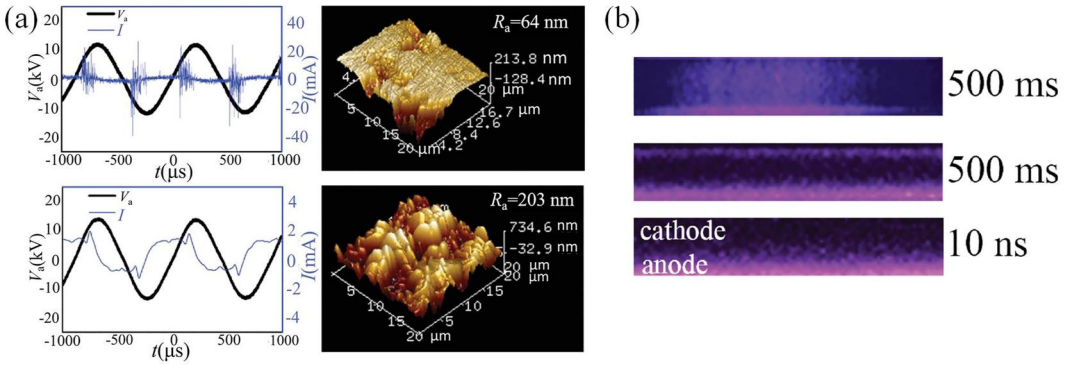

FIGURE 16 (a) Waveforms of the applied voltage V_a, current I, AFM scan of ceramics and (b) the discharge images (500 ms for smooth ceramics, 500 ms and 10 ns for rough ceramics) in 2-mm air at atmospheric pressure, smooth ceramics with average roughness R_a = 64 nm, surface area S_a = 404 μm^2, ceramics with R_a = 203 nm, S_a = 455 μm^2 [101].

From the above investigations, it can be seen that different electrode structures, dielectric barrier materials, and power supplies can affect the discharge process, which results in air DBD with different characteristics and in different modes. At atmospheric pressure, it is more likely to form a filamentary discharge due to the high collisional frequencies and ionisation rates. To control the electron avalanche amplification, it is important to reduce the ionisation coefficient, which increases with the reduced electric field strength. Formation of H-DBD at atmospheric pressure hence needs to be in a low electric field strength and a relatively uniform distribution of the space charge between the interelectrode gaps to avoid electric field distortion. However, in air, due to the quenching of the nitrogen metastable $N_2(A)$ by O_2, Penning ionisation cannot be used for the electron creation to maintain discharge at a low electric field. Consequently, specific electrode structures such as mesh electrodes [68, 87–89] and asymmetric electrical structures with small radius components [97, 99] were designed to produce seed electrons. Some materials such as electret material [68, 87–99] and porous alumina ceramic [21, 100, 101] can also facilitate the seed electron generation in favour of the homogeneous mode. The mechanism for an electret material to generate a homogeneous discharge can be explained as the desorption current density j_{des} of the electret material (on the order of 10^4-10^5 $cm^{-2}s^{-1}$, that is only one electron may be emitted from an area of 1 cm^2 during 10^{-4}-10^{-5} s) is much less than that of an ordinary dielectric barrier material (on the order of 10^{10}-10^{12} $cm^{-2}s^{-1}$) after discharge [95, 104]. Therefore, the remaining charges in the electret material should provide seed electrons for discharge initiation so that the breakdown process can happen at a lower voltage. With large desorption current and minimal overvoltage, a homogeneous discharge can be obtained [95]. The function of the electret material in DBD is illustrated in Figure 18. It shows that after discharge, the charges are injected in electret material or deposited on the material surface in Figure 18a, which results in the discharge extinguishing but enhances the discharge in the next half circle with seed electrons and the extra electric field. Therefore, one of the mechanisms of the formation of air H-DBD is the seed electron generation by the optimisation of the electrode structure and the selection of dielectric barrier materials.

The multilayer and water electrode structure DBDs can limit current as distributed ballasts, thus lower the electric field and prevent the discharge from glow-to-filament transition [96, 98]. The application of nanosecond pulsed power excitation can also prevent the transition from glow to filament by applying steep pulse edges and short pulse durations [90, 93, 104]. Generally, the breakdown voltage of a nanosecond pulsed DBD

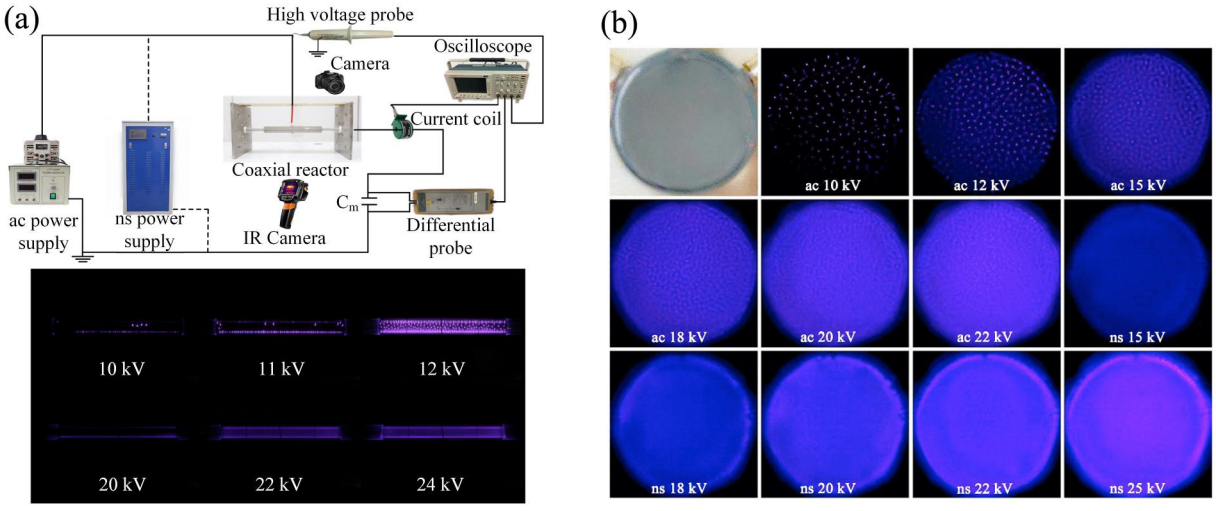

FIGURE 17 Images of the nanosecond-pulsed DBD and the ac DBD at different applied voltages with (a) coaxial DBD structure [104] and (b) plate-plate DBD structure [90].

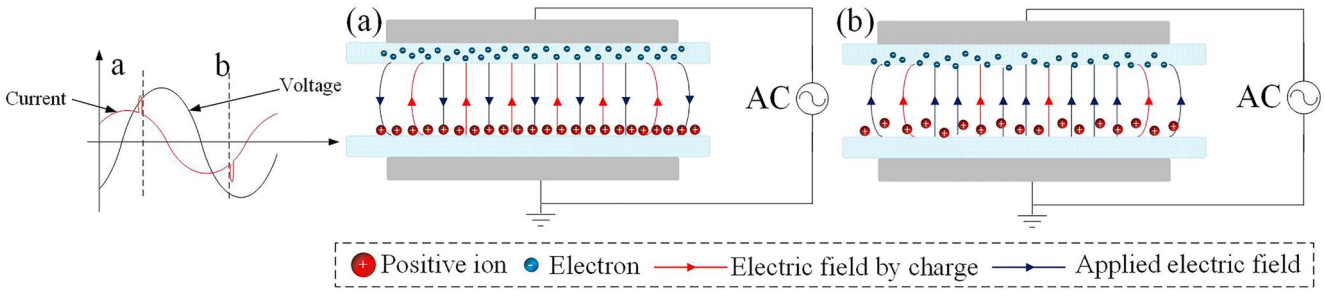

FIGURE 18 Illustration of the function of electret material in DBD (a) after and (b) before discharge.

is much higher than that of an ac DBD, which results in a higher instantaneous electric field and more seed electrons in the gap. At the same time, the application of a short pulse duration prevents the gas heating and reduces the formation of the secondary avalanche and steamers. Figure 19 shows the discharge process of a nanosecond pulsed DBD at the rise and fall edges. During the rising edge of the pulse, Figure 19a shows a simplified charged particle (i.e., positive ions and electrons) motions before the first breakdown discharge occurs in the gap. Under the applied electric field, the gas is ionised, and the ionisation coefficient mainly depends on the electric field strength. Figure 19b is a snapshot of the charged particle distribution when the breakdown discharge is occurring. The electrons are accelerated to the instantaneous anode by the electric field and collide with the ambient molecules along their way, resulting in the electron avalanche. Figure 19c shows that the discharge is soon extinguished after the electron avalanche develops and extends to the entire gas gap, and the internal electric field established in the discharge cancels the external electric field, resulting in insufficient field strength to sustain the discharge. During the falling edge of the pulse, Figure 19d shows the charge distribution before the second breakdown. The residual charges on the dielectric surface and in the gap after the first discharge will affect the discharge process during the pulse falling edge. With the (sudden) decrease of the applied voltage, the reverse electric field due to the surface charges established in the previous process is suddenly enhanced such that the electrons are accelerated towards the other electrode, resulting in the second breakdown. When the second breakdown occurs, similar as the first discharge, the ionisation happens and the electron avalanche develops, as shown in Figure 19e. Figure 19f shows that after the second discharge, the residual charge recombines and dissipates.

Homogeneous discharge in air is still rare in industries despite the efforts made in understanding the mechanisms for air H-DBD in the past decades. For nanosecond pulsed excitation, there are many parameters affecting the discharge process in a synergetic and coupled manner. The lack of the comprehensive studies on the dependence of the nanosecond pulsed DBD formation and mode transition on the related power and gas parameters prevents the application of air H-DBD for industrial uses. Nevertheless, strategies to reduce the electric field distortion, promote the seed electrons production, and lower the breakdown voltage by selecting suitable dielectric materials and power parameters can be helpful. For future industrial applications, more fundamental and systematic studies are needed. Effects of the pulse parameters including pulse rise time, pulse repetition rate and pulse duration on the air H-DBD generation need to be systematically investigated, following examples such as [4, 7]. In addition

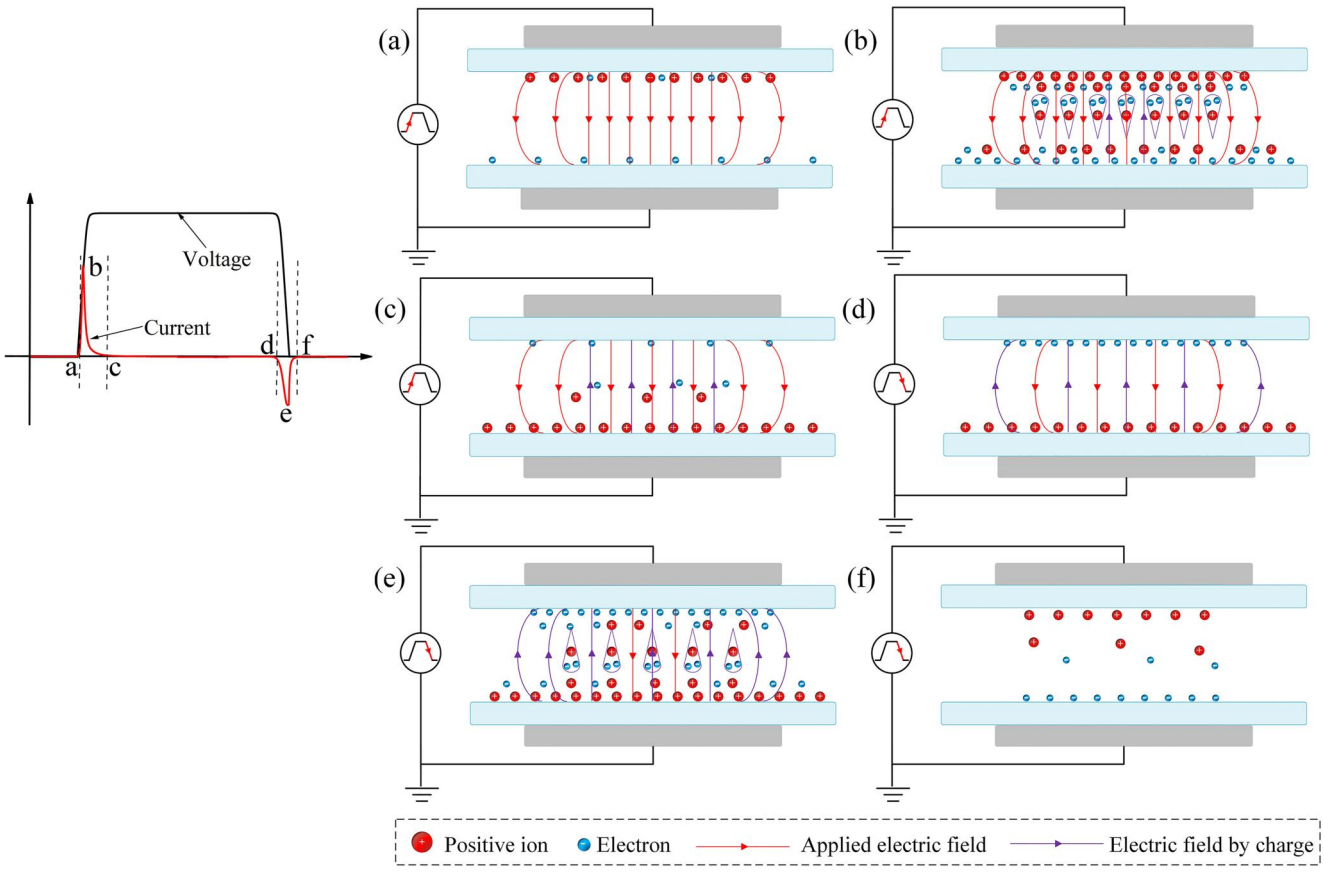

FIGURE 19 Illustration of the discharge processes of a nanosecond pulsed DBD at the pulse rise and fall edges. (a)–(f) Corresponding to the label of (a)–(f) in the current waveform.

to employing advanced diagnostic techniques, simulation modelling is needed for the comprehensive understanding and will expedite the optimisation process for industrial applications.

4 | MULTIPLE-CURRENT-PULSE (MCP) BEHAVIORS IN H-DBD

As mentioned in the previous section, the temporal waveform of atmospheric H-DBD is usually characterised by one narrow current pulse per half cycle of the applied voltage. Such discharge can be called single-current-pulse (SCP) behaviour and was even considered to be related to the homogeneity of DBD during the early study on H-DBDs. In fact, not only SCP behaviour but also multi-current-pulse (MCP) discharge per half cycle has been observed, reported, and investigated in the studies on uncovering the mechanism of H-DBD. Although the MCP discharge seldom occurs in noble gas and nitrogen, it can sometimes appear in helium. In this section, we will briefly introduce the research on MCP behaviours in H-DBD from experimental observations and numerical simulations, respectively.

4.1 | MCP behaviours from experiments

The early observation on the MCP behaviour in homogeneous gas discharges can date back to 1960s when Bartnikas [105] studied the discharge rate and energy loss in helium between metallic-electrodes at atmospheric pressure. Experiments show that at low frequencies (between 20 and 320 Hz) of sinusoidal voltage, the discharge can exhibit two types of mechanisms, namely spark-type and pseudo-glow, with gap-separation extending from 0.05 to 5.0 mm. When the discharge enters the region of pseudo-glow, the MCP behaviour in the presence of small pulses of diminishing magnitude can be observed by examining the voltage waveforms across the gap.

After 2000, when H-DBD attracted more attentions from a variety of fields, reports on MCP behaviours also began to appear in discharges with dielectric barrier. In 2001, Akishev et al. [106] reported the experimental phenomena of periodic current pulsations in H-DBDs in helium at small values of pd (p is gas pressure and d is discharge gap distance, below 500 torr mm) and moderate frequencies of the applied voltage (below 100 kHz). The MCP behaviour here is considered as "pulsed regime of the diffusive mode" of the discharge. A simplified one-dimensional numerical model is developed to investigate the origin of such MCP discharge. Results show that the physical nature of the observed MCPs can be explained in terms of the negative differential resistance of the cathode fall region, which occupies essentially the entire interelectrode gap in each half cycle of the applied voltage. In 2002, Mangolini et al. [107] also presented an experimental investigation on MCP discharge by revealing the radial structure of a low-frequency DBD at atmospheric pressure. From the simultaneously measured radial current distribution and discharge light emission, it is observed that the first current pulse originates in the discharge centre and spreads radially outward, thereby causing a non-uniform surface charge distribution which further results in the second breakdown occurring at first in the discharge periphery. In 2003, Radu et al. [108] reported a similar pseudoglow or multipeak phenomenon in helium as that in Ref. [105] when they experimentally study H-DBD in different noble gases. It is observed that at somewhat lower frequency (2 kHz here) the MCP behaviour appears when the applied voltage is increased. Under the experimental conditions in Ref. [108], as many as eight current pulses per half cycle can be observed as shown in Figure 20. Moreover, in 2003, Shin and Raja [109] found that the pulse current densities decrease and the number of current pulses per half cycle increases as the frequency of the applied voltage decreases as shown in Figure 21. At the experimental conditions of their study, a single pulse at 10 kHz, two pulses at 5 kHz, and five pulses at 1 kHz are observed. They also analysed the formation mechanism of these MCP behaviours and considered them as a consequence of repeated temporally separated (not spatially separated) breakdown events in the discharge.

Considering that impurity is unavoidable in practical applications, in 2010, Martens et al. [110] experimentally investigated the influence of various levels of nitrogen impurity on the electrical performance of H-DBDs in helium at atmospheric pressure. They observed that the MCP discharge occurs when the nitrogen content increases. Specifically, a second breakdown at 3850 ppm of nitrogen and a third breakdown at 4000 ppm are recorded in their study. The key effect of the additional nitrogen is regarded to stimulate Penning ionisation, thereby facilitating volume ionisation and the consequent MCP discharge. In 2017, Bogaczyk et al. [111] also presented a thorough experimental study on the spatio-temporal characterisation of the MCP regime of diffuse DBD in helium with small nitrogen admixtures. They also observed that the number of current pulses per half cycle rises with the increase of nitrogen admixture due to the predominant role of Penning ionisation. Experimental

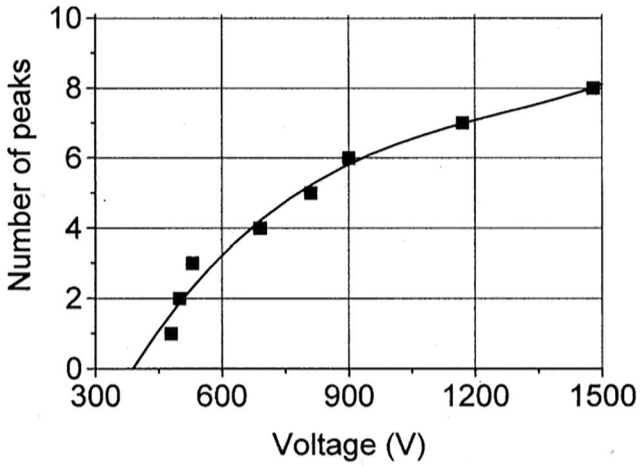

FIGURE 20 Number of current pulses versus the applied voltage [108].

measurement and analysis showed that the transition from the first glow-like breakdown to the last Townsend-like breakdown is favoured by residual species from the former breakdowns which enhance the secondary electron emission during the pre-phase of the later breakdowns. Moreover, the surface charge measurements reveal that the consecutive breakdowns occur alternately at central and peripheral regions on the electrode surface, which is similar as the previous report in Ref. [107]. Sublet et al. [112] observe the apparition of oscillations on the discharge current in nitrogen when the pressure decreases.

4.2 | MCP behaviours from numerical simulations

Inspired by the experimental reports and studies on the MCP behaviour in H-DBDs, the numerical model is developed and utilised to investigate the underlying mechanism which is difficult to get through only by experimental means due to the limitation of diagnostics technique for non-equilibrium atmospheric pressure plasma. To this end, we have to employ the numerical model to simulate the cycle-by-cycle evolution of H-DBDs at different operating parameters and further reveal the in-depth mechanism by analysing the detailed spatio-temporal evolution of main state variables, such as electron density, ion density, and electric field.

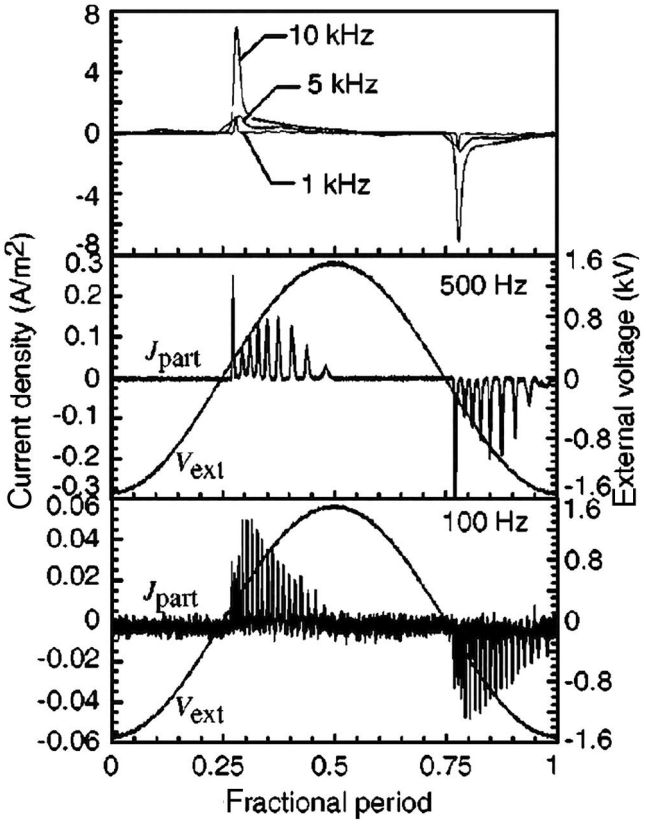

FIGURE 21 Dependence of the current densities and number of current pulses on the frequency of the applied voltage [109].

As early as in 2003, Golubovskii et al. [113] used a one-dimensional fluid model to numerically investigate the spatio-temporal characteristics of the H-DBD in helium. They mainly studied two basic modes of the discharge, namely the Townsend and glow modes. In their numerical study, they found that the Townsend discharge in helium is characterised by small amplitudes of the current and meanwhile by the presence of MCPs during the half cycle. Detailed analysis shows that the MCP behaviour is provided by a lag between the production of ions and resonance atoms nearby the anode and subsequent ion-electron emission and photoemission at the cathode; the damping of the oscillation is caused by the desorption of electrons from the cathode.

In 2005 and 2006, Wang et al. [114, 115] used a similar one-dimensional fluid model to study the MCP behaviour of H-DBD in helium at atmospheric pressure as shown in Figure 22. The effect of the applied voltage amplitude, frequency, as well as the dielectric layer, on the MCP discharge is specifically discussed and analysed. Simulation results show that MCP can be formed in the case of a smaller gap width due to the increase of charge density deposited on dielectric surfaces leading to the enhancement of the induced electric field. In addition, the amplitude and frequency of the applied voltage can also influence the number and the amplitude of current pulses. An interesting finding in Ref. [115] is that both Townsend and glow modes can be observed in a MCP discharge sequence, which is different from that only Townsend discharge presents MCP behaviours in Ref. [113]. In 2008, Zhang et al. [116] further conducted experimental study to verify the numerical findings in Refs. [114, 115]. They emphasised that in one MCP discharge sequence, the next current pulse is always affected by the previous current pulse and breakdown voltage of the second current pulse is usually lower than that of the first one. Moreover, the accumulated charges on the dielectric plate play an important role in promoting the discharge at the beginning and restraining it at the later stage in a MCP discharge sequence.

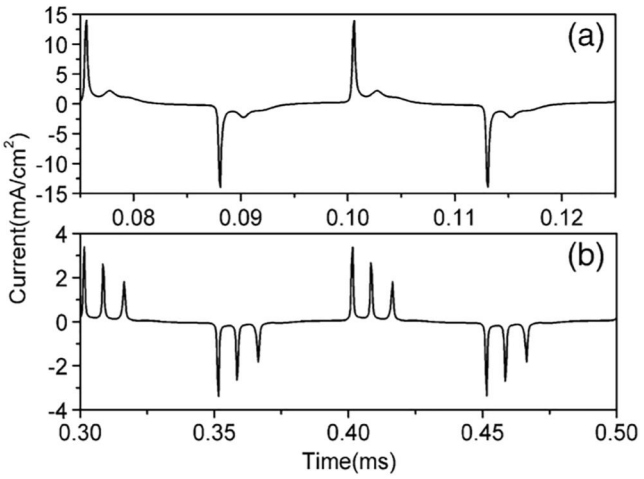

FIGURE 22 Single-current-pulse discharge at 40 kHz (a) and MCP discharge at 10 kHz (b) [115].

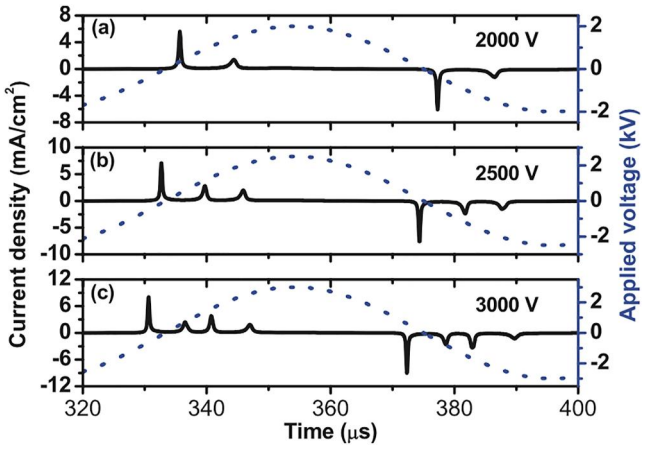

FIGURE 23 MCP discharges at different amplitude of different applied voltages (a) 2000 V, (b) 2500 V, (c) 3000 V [117].

In 2015, Bai et al. [117] began to use two-dimensional fluid model to investigate the radial structure of the MCP discharge as shown in Figure 23. It is worth noting that one-dimensional model, for the sake of simplicity, holds the assumption that the discharge is homogeneous in radial direction; thus, it is not capable of dealing with the numerical study on the radial structure of MCP discharge. Through the two-dimensional model, Bai et al. found that the discharge current densities at different radial positions do not reach their peaks simultaneously, indicating a radial non-uniform structure for the MCP discharge. The time delay between the plasma ignitions in different positions becomes larger in the successive current pulses. It is believed that the edge effect in the first current pulse and the activation-inhibition mechanism in the successive current pulses lead to the radial non-uniformity.

From 2018, Dai's group from South China University of Technology conducted a lot of work on understanding the MCP behaviours in DDBs at atmospheric pressure. In 2018 [118], using one-dimensional fluid model, they reported a systematic investigation on the dynamics and evolution mechanism of MCP behaviour in H-DBD in helium at atmospheric pressure. Similarly, they also found that the MCP discharge can include both Townsend and glow modes. Comparing previous studies, their work revealed more details on the dynamics and evolution as the parameters (the amplitude and the frequency of the applied voltage and gap width) vary. In 2019 [119], they further used the similar one-dimensional fluid model to investigate the influence of nitrogen impurity on the evolution of MCP behaviour in an H-DBD in helium. They observed that the discharge evolves from the MCP mode into a single-pulse mode, and finally returns to the MCP mode when the nitrogen content changes from 0.1 ppm to 10,000 ppm. In particular, they analysed the role of Penning ionisation in the dynamic evolution of discharge at different nitrogen content, thus providing a better understanding on the evolution of MCP discharge from the underlying reactions. In 2020 [120], Dai's group utilised the same numerical model to investigate the influence of oxygen on the MCP behaviour in an atmospheric H-DBD in helium with air impurities. It was found that the oxygen Penning ionisation plays a leading role in the discharge characteristics. As the air content rises from 0 to 5000 ppm, the discharge undergoes a transition from a single-pulse mode to MCP mode, and the number of current pulses also increases. Further analysis also reveals that the rapid growth of direct ionisation prior to the breakdown and the attachment reaction of oxygen both help to generate the MCP discharge at higher air concentration. In 2021, Dai et al. extended their study from the discharge driven by the sinusoidal voltage to the discharge driven by repetitive unipolar narrow pulse [121]. Using the same one-dimensional fluid model, they investigate the effects of applied voltage amplitude, pulse repetition frequency, gap width, and secondary electron emission coefficient on the formation of MCP discharge. An interesting phenomenon, which is never reported in the previous work driven by the sinusoidal voltage, is that under repetitive unipolar pulse excitation, the MCP behaviour will lead to the stratification of electron density distribution in axial direction. Further analysis reveals that the increasing electric field of the cathode fall region is the basis for the formation of MCP behaviour. Based on their fundamental understanding on the formation mechanism of MCP behaviour in H-DBDs, Dai's group also tries to manipulate or control the MCP discharge to avoid the negative influence of MCP discharge in practical applications. In 2019 [122], they reported a systematic numerical study on the control of discharge pulse number in an atmospheric helium DBD. By replacing the original sinusoidal applied voltage with a peak-levelled one, the manipulation of current pulse number in each half cycle is achieved. A preliminary analytical method is also proposed to switch the original MCP discharge into a single-current-pulse discharge. In 2021 [123], they tried to use the multi-frequency pulse-type voltage as the control method to control the number of discharge current pulses. The study is carried out numerically with a one-dimensional fluid model. Results show that the number of current pulses in each half cycle decreases from 5 to 1 as shown in Figure 24, indicating the transition from the MCP discharge to single-current-pulse discharge, when the harmonics N increases from 1 to 11. Finally, an analytical method is also presented to estimate the minimum harmonics required to achieve the targeted single-current-pulse discharge.

5 | CONCLUSION

In conclusion, various parameters such as gas flow, dielectric material properties, surface conductivities, and electrode shape have significant effects on the appearance of DBD. Gas flow can influence the formation of H-DBD by affecting the density of quenchers and seed electrons within the discharge. Dielectric material properties, such as thickness, surface charge, and shallow traps, can also affect the discharge mode. Surface conductivities and electrode shape are additional parameters that can impact the formation of DBD.

The mechanisms of H-DBD formation were reviewed chronologically. The three-condition hypothesis proposed by

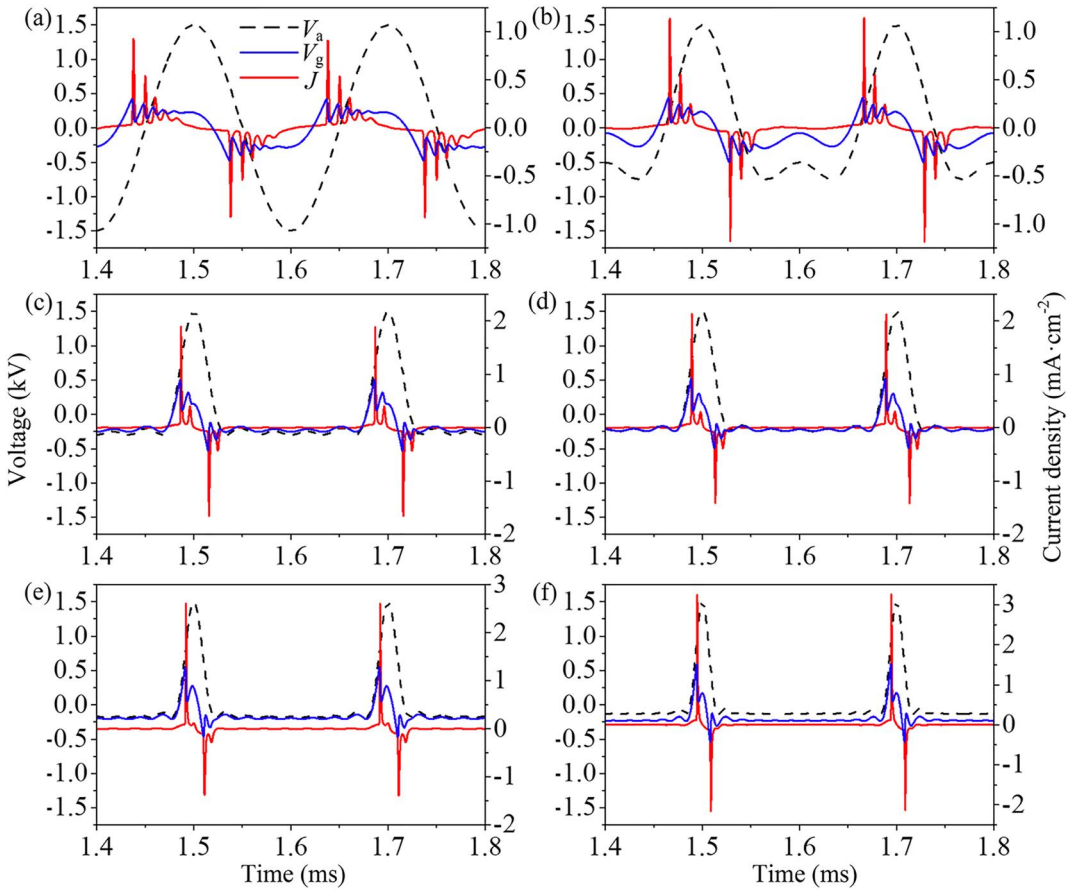

FIGURE 24 Controlling the number of pulses with different values of the harmonics-related parameter N (a) $N = 1$, (b) $N = 2$, (c) $N = 5$, (d) $N = 6$, (e) $N = 8$, and (f) $N = 11$. Here, V_a is the applied voltage; V_g is the gap voltage; J is the discharge current density [123].

Okazaki's group in 1990 was reevaluated and refined by Massines and colleagues in 1998 to be a low breakdown electric field, high residual electron density before ignition of a new discharge, and the use of dielectrics allowing electrons to be trapped in shallow traps of the surface during previous pulses.

The behaviours of N_2 metastable species in N_2 DBD have been extensively studied. Different hypotheses were proposed to explain the generation of H-DBD in N_2. The initial hypothesis of Penning ionisation between two N_2 metastable molecules was later challenged due to the short lifetime of $N_2(a)$, and the addition of Xe to N_2 did not affect the generation of H-DBD. Instead, it was proposed that the flux of $N_2(A)$ to the dielectric surface, which increases the cathode secondary emission coefficient, is responsible for the generation of seed electrons required for H-DBD. The effect of O_2 concentration on the transition from H-DBD to F-DBD was investigated. It was found that higher O_2 concentrations lead to more effective quenching of $N_2(A)$ and promote the transition to F-DBD. But this could not explain the observed significant increase in N_2 second positive system emission when the O_2 concentration was increased from 0 to 40 ppm. Recently, it was proposed that the associative ionisation reaction between $N(^2P)$ and $O(^3P)$ is responsible for the seed electron. Overall, the understanding of N_2 metastable species and their roles in DBD behaviour is still an active area of research, and more studies are needed to fully elucidate the underlying mechanisms. For example, all these cannot explain that H-DBD can also be obtained in the air under certain conditions.

The generation of H-DBD in the air is influenced by various factors, including the electrode structure, dielectric material, and pulse power supplies. Understanding and optimising these factors can help achieve a stable and uniform discharge pattern, which is important for the industrial applications of H-DBD in the air. Further research and development in these areas may lead to improved techniques for generating H-DBD in the air with enhanced performance and efficiency.

Nevertheless, to generate H-DBD, seed electrons are favourable, which can be due to different mechanisms. However, how many roles each mechanism plays is still not clearly understood. Recently, Bajon et al. [124] reported a T-DBD generated in CO_2, and this is something interesting that might be also helpful for understanding the generation of H-DBD.

The study of multiple-current-pulse (MCP) behaviours in homogeneous dielectric barrier discharges (H-DBDs) has shown that MCPs can occur in atmospheric pressure plasma with different gases, electrode configurations, and applied voltages. Experimental observations and numerical

simulations have provided insights into the mechanisms underlying MCP behaviours in H-DBDs. MCPs have been observed at different frequencies of the applied voltage and discharge gap distances and can be related to phenomena such as negative differential resistance of the cathode fall region, radial current distribution, surface charge distribution, and impurity effects. Numerical simulations have been useful in understanding the underlying mechanisms of MCP behaviours, which are difficult to investigate solely through experimental means due to limitations in diagnostics techniques. Overall, the study of MCP behaviours in H-DBDs has contributed to a better understanding of the complex dynamics of atmospheric pressure plasma and can have implications for the design and optimisation of DBD-based plasma devices for various practical applications.

ACKNOWLEDGEMENT

Efforts of X. Lu are supported by the National Natural Science Foundation of China (Grant Nos. 52130701, 51977096, and 12005076) and National Key Research and Development Program of China (Grant No. 2021YFE0114700). Effort of C. Jiang is supported by the Air Force Office of Scientific Research of the United States of America (Grant Nos FA9550-22-1-0115 and FA9550-22-1-0428).

CONFLICT OF INTEREST STATEMENT

None.

DATA AVAILABILITY STATEMENT

Data sharing not applicable—no new data generated.

ORCID

Xinpei Lu https://orcid.org/0000-0003-0676-9585
Tao Shao https://orcid.org/0000-0002-5738-1241
Cheng Zhang https://orcid.org/0000-0003-1512-2820
Dawei Liu https://orcid.org/0000-0003-3503-2099

REFERENCES

1. Domonkos, M., et al.: Applications of cold atmospheric pressure plasma technology in medicine, agriculture and food industry. Appl. Sci. Basel 11(11), 4809 (2021)
2. Yan, D., Sherman, J.H., Keidar, M.: Cold atmospheric plasma, a novel promising anti-cancer treatment modality. Oncotarget 8(9), 15977–15995 (2017)
3. Jin, S., et al.: A non-equal gap distance dielectric barrier discharge: between cone-shape and cylinder-shape electrodes. High Volt. 7(1), 98–105 (2022)
4. Nijdam, S., Teunissen, J., Ebert, U.: The physics of streamer discharge phenomena. Plasma Sources Sci. Technol. 29(10), 103001 (2020)
5. Jiang, C., et al.: Removal of volatile organic compounds in atmospheric pressure air by means of direct current glow discharges. IEEE Trans. Plasma Sci. 33(4), 1416–1425 (2005)
6. Jiang, C., et al.: Pulsed atmospheric-pressure cold plasma for endodontic disinfection. IEEE Trans. Plasma Sci. 37(7), 1190–1195 (2009)
7. Zhang, S., et al.: Dry reforming of methane by microsecond pulsed dielectric barrier discharge plasma: optimizing the reactor structures. High Volt. 7(4), 718–729 (2022)
8. Neyts, E., Bogaerts, A.: Understanding plasma catalysis through modelling and simulation-a review. J. Phys. D Appl. Phys. 47(22), 224010 (2014)
9. Peng, B., et al.: Streamer dynamics and charge self-erasing of two counter-propagating plasmas in repetitively pulsed surface dielectric barrier discharge. High Volt. 7(4), 730–743 (2022)
10. Kogelschatz, U.: Filamentary, patterned, and diffuse barrier discharges. IEEE Trans. Plasma Sci. 30(4), 1400–1408 (2002)
11. Kogelschatz, U.: Dielectric-barrier discharges: their history, discharge physics, and industrial applications. Plasma Chem. Plasma Process. 23(1), 1–46 (2003)
12. Peng, S., et al.: Oxidative modifications and structural changes of human serum albumin in response to air dielectric barrier discharge plasma. High Volt. 6(5), 813–821 (2021)
13. Fridman, A., Chirokov, A., Gutsol, A.: Non-thermal atmospheric pressure discharges. J. Phys. D Appl. Phys. 38(2), R1–R24 (2005)
14. Ito, M., et al.: Current status and future prospects of agricultural applications using atmospheric-pressure plasma technologies. Plasma Process. Polym. 15(2), e1700073 (2018)
15. Bruggeman, P., Brandenburg, R.: Atmospheric pressure discharge filaments and microplasmas: physics, chemistry and diagnostics. J. Phys. D Appl. Phys. 46, 464001 (2013)
16. Nersisyan, G., Graham, W.: Characterization of a dielectric barrier discharge operating in an open reactor with flowing helium. Plasma Sources Sci. Technol. 13(4), 582–587 (2004)
17. Weltmann, K.-D., Woedtke, T.V.: Plasma medicine - current state of research and medical application. Plasma Phys. Control Fusion 59(1), 014031 (2017)
18. Ramakers, M., et al.: Effect of argon or helium on the CO_2 conversion in a dielectric barrier discharge. Plasma Process. Polym. 12(8), 755–763 (2015)
19. Bruggeman, P.J., Iza, F., Brandenburg, R.: Foundations of atmospheric pressure non-equilibrium plasmas. Plasma Sources Sci. Technol. 26(12), 123002 (2017)
20. Geyter, N., Morent, R., Leys, C.: Surface modification of a polyester non-woven with a dielectric barrier discharge in air at medium pressure. Surf. Coat. Technol. 201, 2460–2466 (2006)
21. Ran, J., et al.: Homogeneous dielectric barrier discharges in atmospheric air and its influencing factor. Phys. Plasmas 25(3), 033511 (2018)
22. Yu, S., et al.: Study on the mode-transition of nanosecond-pulsed dielectric barrier discharge between uniform and filamentary by controlling pressures and pulse repetition frequencies. Phys. Plasmas 23(2), 023510 (2016)
23. Pekarek, S.: Experimental study of surface dielectric barrier discharge in air and its ozone production. J. Phys. D Appl. Phys. 45(7), 075201 (2012)
24. Ono, R., Oda, T.: Ozone production process in pulsed positive dielectric barrier discharge. J. Phys. D Appl. Phys. 40(1), 176–182 (2007)
25. Siemens, W.: Ueber die elektrostatische Induction und die Verzögerung des Stroms in Flaschendrähten. Ann. Phys. 178(9), 66–122 (1857)
26. Eliasson, B., Egli, W., Kogelschatz, U.: Modelling of dielectric barrier discharge chemistry. Pure Appl. Chem. 66(6), 1275–1286 (1994)
27. Mildren, R., Carman, R.: Enhanced performance of a dielectric barrier discharge lamp using short-pulsed excitation. J. Phys. Appl. Phys. 34(1), L1–L6 (2001)
28. Kogelschatz, U.: Silent discharges for the generation of ultraviolet and vacuum ultraviolet excimer radiation. Pure Appl. Chem. 62(9), 1667–1674 (1990)
29. Fridman, G., et al.: Blood coagulation and living tissue sterilization by floating-electrode dielectric barrier discharge in air. Plasma Chem. Plasma Process. 26(4), 425–442 (2006)
30. Weltmann, K.-D., et al.: The future for plasma science and technology. Plasma Process. Polym. 16(1), 1800118 (2019)
31. Tu, X., Whitehead, J., et al.: Plasma-catalytic dry reforming of methane in an atmospheric dielectric barrier discharge: understanding the synergistic effect at low temperature. Appl. Catal. B-Environmental. 125, 439–448 (2012)
32. Mei, D., et al.: Plasma-assisted conversion of CO_2 in a dielectric barrier discharge reactor: understanding the effect of packing materials. Plasma Sources Sci. Technol. 24(1), 015011 (2015)

33. Pavlovich, M., et al.: Ozone correlates with antibacterial effects from indirect air dielectric barrier discharge treatment of water. J. Phys. D Appl. Phys. 46(14), 145202 (2013)
34. Boeuf, J., Pitchford, L.C.: Electrohydrodynamic force and aerodynamic flow acceleration in surface dielectric barrier discharge. J. Appl. Phys. 97(10), 103307 (2005)
35. Morent, R., et al.: Study of the ageing behaviour of polymer films treated with a dielectric barrier discharge in air, helium and argon at medium pressure. Surf. Coating Technol 201(18), 7847–7854 (2007)
36. Corke, T., Enloe, C.L., Wilkinson, S.P.: Dielectric barrier discharge plasma actuators for flow control. Annu. Rev. Fluid Mech. 42(1), 505–529 (2010)
37. Brandenburg, R.: Dielectric barrier discharges: progress on plasma sources and on the understanding of regimes and single filaments. Plasma Sources Sci. Technol. 26(5), 053001 (2017)
38. Kanazawa, S., et al.: Stable glow plasma at atmospheric pressure. J. Phys. D Appl. Phys. 21(5), 838–840 (1988)
39. Massines, F., et al.: Experimental and theoretical study of a glow discharge at atmospheric pressure controlled by dielectric barrier. J. Appl. Phys. 83(6), 2950–2957 (1998)
40. Massines, F., Gouda, G.: A comparison of polypropylene-surface treatment by filamentary, homogeneous and glow discharges in helium at atmospheric pressure. J. Phys. D Appl. Phys. 31(24), 3411–3420 (1998)
41. Massines, F., et al.: The role of dielectric barrier discharge atmosphere and physics on polypropylene surface treatment. Plasmas Polym. 6, 35 (2001)
42. Gherardi, N., Martin, S., Massines, F.: A new approach to SiO_2 deposit using a N_2-SiH_4-N_2O glow dielectric barrier-controlled discharge at atmospheric pressure. J. Phys. D Appl. Phys. 33(19), L104–(2000)
43. Montie, T.C., Kelly-Wintenberg, K., Roth, J.R.: An overview of research using the one atmosphere uniform glow discharge plasma (OAUGDP)for sterilization of surfaces and materials. IEEE Trans. Plasma Sci. 28(1), 41–50 (2000)
44. Roth, J.R., Sherman, D.M., Wilkinson, S.P.: Electrohydrodynamic flow control with a glow-discharge surface plasma. AIAA J. 38(7), 1166–1172 (2000)
45. Roth, J.R.: Aerodynamic flow acceleration using paraelectric and peristaltic electrohydrodynamic effects of a One Atmosphere Uniform Glow Discharge Plasma. Phys. Plasmas 10(5), 2117–2126 (2003)
46. Naseh, M.V., et al.: Fast and clean functionalization of carbon nanotubes by dielectric barrier discharge plasma in air compared to acid treatment. Carbon 48(5), 1369–1379 (2010)
47. Sivachandiran, L., Khacef, A.: Enhanced seed germination and plant growth by atmospheric pressure cold air plasma: combined effect of seed and water treatment. RSC Adv. 7(4), 1822–1832 (2017)
48. Shang, K.F., et al.: Synergetic degradation of Acid Orange 7 (AO7) dye by DBD plasma and persulfate. Chem. Eng. J. 311, 378–384 (2017)
49. Tian, W., Kushner, M.J.: Atmospheric pressure dielectric barrier discharges interacting with liquid covered tissue. J. Phys. D Appl. Phys. 47(16), 165201 (2014)
50. Kalghatgi, S.U., et al.: Mechanism of blood coagulation by nonthermal atmospheric pressure dielectric barrier discharge plasma. IEEE Trans. Plasma Sci. 35(5), 1559–1566 (2007)
51. Ayan, H., et al.: Nanosecond-pulsed uniform dielectric-barrier discharge. IEEE Trans. Plasma Sci. 36(2), 504–508 (2008)
52. Daeschlein, G., et al.: In vitro susceptibility of multidrug resistant skin and wound pathogens against low temperature atmospheric pressure plasma jet (APPJ) and dielectric barrier discharge plasma (DBD). Plasma Process. Polym. 11(2), 175–183 (2014)
53. Babaeva, N.Y., Kushner, M.J.: Reactive fluxes delivered by dielectric barrier discharge filaments to slightly wounded skin. J. Phys. D Appl. Phys. 46(2), 025401 (2013)
54. Osawa, N., et al.: Comparison of the ozone generation efficiency by two different discharge modes of dielectric barrier discharge. Eur. Phys. J. Appl. Phys. 55(1), 13802 (2011)
55. Luo, H., et al.: Characteristics of shallow traps in the dielectric surface and their effects on diffuse dielectric barrier discharge in air. IEEE Trans. Plasma Sci. 45(5), 749–753 (2017)
56. Ran, J., et al.: Homogeneous dielectric barrier discharges in atmospheric air and its influencing factor. Phys. Plasmas 25(3), 033511 (2018)
57. RanZhang, J.X., et al.: Effect of dielectric surface morphology on dielectric barrier discharge mode in air at atmospheric pressure. IEEE Trans. Plasma Sci. 49(1), 214–218 (2021)
58. Belinger, A., Dap, Si., Naude, N.: Influence of the dielectric thickness on the homogeneity of a diffuse dielectric barrier discharge in air. J. Phys. D Appl. Phys. 55(46), 465201 (2022)
59. Garamoon, A.A., et al.: Influences of the barrier types and arrangements on dielectric barrier discharge characteristics. Eur. Phys. J. Appl. Phys. 53(2), 21001 (2011)
60. Yao, J., et al.: Asymmetric discharges of dielectric barrier discharge in atmospheric air. Appl. Phys. Lett. 122(8), 082905 (2023)
61. Massines, F., et al.: Recent advances in the understanding of homogeneous dielectric barrier discharges. Eur. Phys. J. Appl. Phys. 47(2), 22805 (2009)
62. Gherardi, N., Massines, F.: Mechanisms controlling the transition from glow silent discharge to streamer discharge in nitrogen. IEEE Trans. Plasma Sci. 29(3), 536–544 (2001)
63. Luo, H.Y., et al.: Homogeneous dielectric barrier discharge in nitrogen at atmospheric pressure. J. Phys. D Appl. Phys. 43(15), 155201 (2010)
64. Li, M., et al.: Effect of surface charge trapping on dielectric barrier discharge. Appl. Phys. Lett. 92(3), 031503 (2008)
65. Li, C.R., et al.: Dielectric barrier discharge using corona-modified silicone rubber. EPL 84(2), 25002 (2008)
66. Mu, H.B., et al.: Effect of aluminum nitride on discharge mode transition in atmospheric pressure He/O_2 DBD. IEEE Trans. Plasma Sci. 46(4), 888–894 (2018)
67. Naudé, N., Massines, F.: Influence of the surface conductivity on the stability of a glow dielectric-barrier discharge. IEEE Trans. Plasma Sci. 36(4), 1322–1323 (2008)
68. Okazaki, S., et al.: Appearance of stable glow discharge in air, argon, oxygen and nitrogen at atmospheric pressure using a 50 Hz source. J. Phys. D Appl. Phys. 26(5), 889–892 (1993)
69. Trunec, D., Brablec, A., Stastny, F.: Experimental study of atmospheric pressure glow discharge. Contrib. Plasma Phys. 38(3), 435–445 (1998)
70. Wang, X.X., et al.: Influence of wire mesh electrodes on dielectric barrier discharge. Plasma Sources Sci. Technol. 15(4), 845–848 (2006)
71. Yokoyama, T., et al.: The mechanism of the stabilisation of glow plasma at atmospheric pressure. J. Phys. D Appl. Phys. 23(8), 1125–1128 (1990)
72. Okazaki, S., Kogoma, M., Uchiyama, H.: Proceedings of the 3rd International Symposium on High Pressure Low Temperature Plasma Chemistry. HAKONE III, Strasbourg, pp. 101 (1991)
73. Massines, F., et al.: Physics and chemistry in a glow dielectric barrier discharge at atmospheric pressure: diagnostics and modelling. Surf. Coating. Technol. 8, 174–175 (2003)
74. Tochikubo, F., Chiba, T., Watanabe, T.: Structure of low-frequency helium glow discharge at atmospheric pressure between parallel plate dielectric electrodes. Jpn. J. Appl. Phys. 38(9R), 5244 (1999)
75. Phelps, A.V.: Absorption studies of helium metastable atoms and molecules. Phys. Rev. 99(4), 1307–1313 (1955)
76. Stevefelt, J., Pouvesle, J.M., Bouchoule, A.: Reaction kinetics of a high pressure helium fast discharge afterglow. J. Chem. Phys. 76(8), 4006–4015 (1982)
77. Gherardi, N., et al.: Transition from glow silent discharge to microdischarges in nitrogen gas. Plasma Sources Sci. Technol. 9(3), 340–346 (2000)
78. Piper, L.G., Cowles, L.M., Rawlins, W.T.: State-to-state excitation of NO($A\ ^2\Sigma^+$, v'=0,1,2) by N_2($A\ ^3\Sigma^+_u$, v'=0,1,2). J. Chem. Phys. 85(6), 3369–3378 (1986)
79. Piper, L.G., Caledonia, G.E., Kennealy, J.P.: Rate constants for deactivation of $N_2(A^3\Sigma+u, v' = 0,1)$ by O. J. Chem. Phys. 75(6), 2847–2852 (1981)
80. Black, G., Sharpless, R.L., Slanger, T.G.: Collision-induced emission from O(^{1}S) by He, Ar, N_2, H_2, Kr, and Xe. J. Chem. Phys. 63(10), 4546–4550 (1975)

81. Kossyi, I.A., et al.: Kinetic scheme of the non-equilibrium discharge in nitrogen-oxygen mixtures. Plasma Sources Sci. Technol. 1(3), 207–220 (1992)
82. Kozlov, K.V., et al.: Investigation of the filamentary and diffuse mode of barrier discharges in N_2/O_2 mixtures at atmospheric pressure by cross-correlation spectroscopy. J. Phys. D Appl. Phys. 38(4), 518–529 (2005)
83. Dilecce, G., Ambrico, P.F., Benedictis, S.D.: $N_2(A\ ^3\Sigma^+_u)$ density measurement in a dielectric barrier discharge in N_2 and N_2 with small O_2 admixtures. Plasma Sources Sci. Technol. 16(3), 511–522 (2007)
84. Brandenburg, R., et al.: Diffuse barrier discharges in nitrogen with small admixtures of oxygen: discharge mechanism and transition to the filamentary regime. J. Phys. D Appl. Phys. 38(13), 2187–2197 (2005)
85. Tyl, C., et al.: Investigation of memory effect in atmospheric pressure dielectric barrier discharge in nitrogen with small oxygen or nitric oxide addition. J. Phys. D Appl. Phys. 51(35), 354001 (2018)
86. Roth, J.R., et al.: The physics and phenomenology of One Atmosphere Uniform Glow Discharge Plasma (OAUGDP™) reactors for surface treatment applications. J. Phys. D Appl. Phys. 38(4), 555–567 (2005)
87. Tepper, J., Lindmayer, M.: International Symposium on High Pressure Low Temperature Plasma Chemistry, vol. 1, pp. 38. HAKONE VII. Greifswald, Germany (2000)
88. Fang, Z., Qiu, Y., Luo, Y.: Surface modification of polytetrafluoroethylene film using the atmospheric pressure glow discharge in air. J. Phys. D Appl. Phys. 36(23), 2980–2985 (2003)
89. Buchta, J., Brablec, A., Trunec, D.: Comparison of ozone production in atmospheric pressure glow discharge and silent discharge. Czech. J. Phys. 50(S3), 273 (2000)
90. Jiang, H., et al.: Comparison of AC and nanosecond-pulsed DBDs in atmospheric air. IEEE Trans. Plasma Sci. 39(11), 2076–2077 (2011)
91. Fang, Z., et al.: Study on the microsecond pulse homogeneous dielectric barrier discharges in atmospheric air and its influencing factors. Plasma Sci. Technol. 13(6), 676–681 (2011)
92. Wu, S., et al.: Dynamics of mode transition in air dielectric barrier discharge by controlling pressures. IEEE Trans. Plasma Sci. 42(10), 2342–2343 (2014)
93. Yang, D., et al.: A homogeneous dielectric barrier discharge plasma excited by a bipolar nanosecond pulse in nitrogen and air. Plasma Sources Sci. Technol. 21(3), 035004 (2012)
94. Fang, Z., et al.: Factors influencing the existence of the homogeneous dielectric barrier discharge in air at aspheric pressure. J. Phys. D Appl. Phys. 40(5), 1401–1407 (2007)
95. Golubovskii, Y.B., et al.: Study of the homogeneous glow-like discharge in nitrogen at atmospheric pressure. J. Phys. D Appl. Phys. 37, 1346 (2004)
96. Shao, T., et al.: A comparative study of water electrodes versus metal electrodes for excitation of nanosecond-pulse homogeneous dielectric barrier discharge in open air. IEEE Trans. Plasma Sci. 41(10), 3069–3078 (2013)
97. Liu, W., et al.: Generation of atmospheric-pressure homogeneous dielectric barrier discharge in air. EPL 118(4), 45001 (2017)
98. Li, J., et al.: Research on homogeneous multilayer DBD driven by submicrosecond pulsed power at atmospheric pressure air. IEEE Trans. Plasma Sci. 46(1), 2–7 (2018)
99. Cui, W., et al.: Influence of non-uniform electric field distribution on the atmospheric pressure air dielectric barrier discharge. Plasma Sci. Technol. 23(7), 075402 (2021)
100. Osawa, N., Yoshioka, Y.: Generation of low-frequency homogeneous dielectric barrier discharge at atmospheric pressure. IEEE Trans. Plasma Sci. 40(1), 2–8 (2011)
101. Ran, J., et al.: Effect of dielectric surface morphology on dielectric barrier discharge mode in air at atmospheric pressure. IEEE Trans. Plasma Sci. 49(1), 214–218 (2020)
102. Zhang, S., et al.: The influencing factors of nanosecond pulse homogeneous dielectric barrier discharge in air. Spectrochim. Acta Mol. Biomol. Spectrosc. 117, 535–540 (2014)
103. Wang, X., et al.: Study on an atmospheric pressure glow discharge. Plasma Sources Sci. Technol. 12(3), 358–361 (2003)
104. Wang, Q., et al.: Investigation on discharge characteristics of a coaxial dielectric barrier discharge reactor driven by AC and ns power sources. Plasma Sci. Technol. 20(3), 035404 (2018)
105. Bartnikas, R.: Discharge rate and energy loss in helium at low frequencies. Arch. Elektrotechnik 52(6), 348–359 (1969)
106. Akishev, Y.S., et al.: Pulsed regime of the diffusive mode of a barrier discharge in helium. Plasma Phys. Rep. 27(2), 164–171 (2001)
107. Mangolini, L., et al.: Radial structure of a low-frequency atmospheric-pressure glow discharge in helium. Appl. Phys. Lett. 80(10), 1722–1724 (2002)
108. Radu, I., et al.: Diagnostics of dielectric barrier discharges in noble gases: atmospheric pressure glow and pseudoglow discharges and spatio-temporal patterns. IEEE Trans. Plasma Sci. 31(3), 411–421 (2003)
109. Shin, J., Raja, L.L.: Dynamics of pulse phenomena in helium dielectric-barrier atmospheric-pressure glow discharges. J. Appl. Phys. 94(12), 7408–7415 (2003)
110. Martens, T., et al.: The influence of impurities on the performance of the dielectric barrier discharge. Appl. Phys. Lett. 96(9), 091501 (2010)
111. Bogaczyk, M., et al.: Spatio-temporal characterization of the multiple current pulse regime of diffuse barrier discharges in helium with nitrogen admixtures. J. Phys. D Appl. Phys. 50(41), 415202 (2017)
112. Sublet, A., et al.: Atmospheric and sub-atmospheric dielectric barrier discharges in helium and nitrogen. Plasma Sources Sci. Technol. 15(4), 627–634 (2006)
113. Golubovskii, Y.B., et al.: Modelling of the homogeneous barrier discharge in helium at atmospheric pressure. J. Phys. D Appl. Phys. 36(1), 39–49 (2003)
114. Wang, Y.H., Wang, D.Z.: Study on homogeneous multiple-pulse barrier discharge at atmospheric pressure. Acta Phys. Sinca. 54(3), 1295–1300 (2005)
115. Wang, D.Z., Wang, Y.H., Liu, C.S.: Multipeak behavior and mode transition of a homogeneous barrier discharge in atmospheric pressure helium. Thin Solid Film 507, 384–388 (2006)
116. Zhang, Y., et al.: Multiple current peaks and mode conversion of atmospheric pressure glow dielectric barrier discharge in helium. Thin Solid Film 516(21), 7547–7554 (2008)
117. Bai, Z.G., Wang, X., Liu, F.: Radial structures of atmospheric-pressure glow discharges with multiple current pulses in helium. J. Phys. D Appl. Phys. 48(34), 345201 (2015)
118. Zhang, Y.H., Ning, W.J., Dai, D.: Numerical investigation on the dynamics and evolution mechanisms of multiple-current-pulse behavior in homogeneous helium dielectric-barrier discharges at atmospheric pressure. AIP Adv. 8(3), 035008 (2018)
119. Zhang, Y.H., Ning, W.J., Dai, D.: Influence of nitrogen impurities on the performance of multiple-current-pulse behavior in a homogeneous helium dielectric-barrier discharges at atmospheric pressure. J. Phys. D Appl. Phys. 52(4), 045203 (2019)
120. Luo, L., et al.: Influence of oxygen on the multiple-current-pulse behavior in an atmospheric homogeneous helium dielectric barrier discharge with air impurities. IEEE Access 8, 8145–8156 (2020)
121. Zhou, X.Y., et al.: Multiple current peaks and spatial characteristics of atmospheric helium dielectric barrier discharges with repetitive unipolar narrow pulse excitation. Plasma Sci. Technol. 23(6), 064003 (2021)
122. Zhang, Y.H., et al.: Manipulating the discharge pulse number in an atmospheric helium dielectric barrier discharge with multiple current pulses per half cycle. Plasma Sources Sci. Technol. 28(10), 104001 (2019)
123. Huang, Z.E., et al.: Controlling the number of discharge current pulses in an atmospheric dielectric barrier discharge by voltage waveform tailoring. AIP Adv. 11(1), 015203 (2021)
124. Bajon, C., et al.: Homogeneous dielectric barrier discharge in CO_2. Plasma Sources Sci. Technol. 32(4), 045012 (2023)

How to cite this article: Lu, X., et al.: On the chronological understanding of the homogeneous dielectric barrier discharge. High Voltage. 8(6), 1132–1150 (2023). https://doi.org/10.1049/hve2.12382